



# Transferring the paired-catchment approach to the subsurface: new insights into the transport and spatiotemporal dynamics of contaminants in an active karst conduit system

Yanina K. Mueller<sup>1</sup> · Nadine Goeppert<sup>1,2</sup> · Nico Goldscheider<sup>1</sup>

Received: 23 October 2024 / Accepted: 27 September 2025  
© The Author(s) 2025

## Abstract

Impacts of land use activities on the water quality of a large karst spring (Blautopf, Germany) were identified by extensive spatiotemporal water quality analysis, and for the first time, a paired-catchment approach was successfully transferred to a subsurface karst and cave system. Water quality changes in karst springs are often rapid, strong, and influenced by a number of factors. This comprehensive study was performed by means of long-term (30-month) monitoring, intensive sampling during a rainfall event, and spatial sampling across the cave system. The spring showed moderate seasonal variations for most parameters but a strong response to the rainfall event, where fecal bacteria (*E. coli*) increased 120-fold, with a most probable number (MPN) of up to 17,168 per 100 mL. The catchment area (165 km<sup>2</sup>) was subdivided into two sub-catchments of similar size and morphology but differing in land use. The subsurface paired-catchment approach demonstrated that major ions, trace elements, rare earth elements and fecal bacteria differed significantly between both sub-catchments and could be attributed to different land use activities. Nitrate was linked to agriculture, whereas potassium, chloride, gadolinium, and fecal bacteria could be identified as indicators for wastewater effluents. Significant influences on water quality included winter application of road salt, (potential) sewer overflows and, to a lesser extent, nitrogen fertilization. This study underlines the susceptibility of karst springs to contamination and demonstrates the applicability of a subsurface paired-catchment approach as a promising tool to identify spatially resolved impacts of land use activities to a karst aquifer.

**Keywords** Karst · Groundwater monitoring · Paired-catchment approach · Natural tracers · Land use

## Introduction

Karst aquifers provide drinking water for 678 million (9.2%) people globally (Stevanović 2019). Karst systems also provide a range of ecosystem services, such as a natural CO<sub>2</sub> sink as well as surface and subsurface biodiversity (Goldscheider 2019). These heterogeneous aquifers are characterized by large fissures and conduits that develop over time, mainly in carbonate and evaporite rocks, due to chemical

dissolution. Large cave systems can form in karst aquifers which collect infiltrated water from the surface and surrounding rock matrix in cave streams that discharge to springs. Rapid infiltration of rain water and high subsurface flow rates are typical for karst systems. This results in high variability in discharge and water quality, as there is only limited filtration of contaminants (Bakalowicz 2005; Gutiérrez et al. 2014; Goldscheider 2019). Many karst aquifers are characterized by long periods of good water quality, which are, however, interrupted by short-term contamination events, often associated with heavy rainfall events that lead to increased mobilization, infiltration, and transport of contaminants (Vesper et al. 2001; Pronk et al. 2007; Long et al. 2012; Frank et al. 2022).

A detailed understanding of water quality changes and the respective origin of contaminations are crucial for a sustainable management of karst springs (Andreo et al. 2006). To observe annual changes, springs are often sampled over

✉ Yanina K. Mueller  
yanina.mueller@kit.edu

<sup>1</sup> Institute of Applied Geosciences, Division of Hydrogeology, Karlsruhe Institute of Technology (KIT), Kaiserstr. 12, 76131 Karlsruhe, Germany

<sup>2</sup> Institute of Geological Sciences, Division of Hydrogeology, Free University Berlin, Malteserstr. 74-100, 12249 Berlin, Germany

large, e.g., monthly, intervals. For investigations of small and rapid changes, which are typical for karst springs, a high-resolution monitoring reveals deeper insights (Huebsch et al. 2014). A major factor regarding input of contaminants into karst aquifers is the land use in the catchment area. For assessing the impact of different land use activities on the water yield and water quality of streams, the paired-catchment approach has been developed. Two proximate catchments that are similar in regard to slope, soils, area, and climate are chosen. If these catchments differ in one aspect (e.g., vegetation or land use), the effect can be directly related to the water yield or quality (Hibbert 1967; Brown et al. 2005; Neary 2016). Paired-catchment approaches have been applied to a range of aquifers, surface streams as well as reservoirs and remain relevant in current hydrogeology research (e.g., Salavati et al. 2016; Hankin et al. 2021; Bai et al. 2024). However, up to now there are only few paired-catchment studies conducted in karst aquifers (Zhao et al. 2010; Sun et al. 2013; Smith et al. 2020).

Groundwater chemistry and geochemical parameters such as major ions, trace elements and rare earth elements (REE) can be used to characterize aquifers in regard to hydrological and geochemical processes as well as anthropogenic influences (Zhao et al. 2010; Jiang et al. 2021; Tran et al. 2023).

The following paragraphs introduce key parameters for water quality monitoring in karst systems: the specific electrical conductivity (EC) of water delivers a valuable indication of changing water quality and hydraulic processes in karst aquifers, such as dilution or piston effect following precipitation events (Ravbar et al. 2011). Chloride ( $\text{Cl}^-$ ) in groundwater has various natural and anthropogenic sources, e.g., in snow-influenced (karst) catchments, it is often related to the application of road salt and can therefore be used as a tracer for anthropogenic influence with a relatively well-known spatial and temporal input function (Robinson and Hasenmueller 2017). High levels of nitrate ( $\text{NO}_3^-$ ) in groundwater, on the other hand, are often linked to chemical fertilizers, soil organic nitrogen, manure, or sewage (Wang et al. 2020; Zhang et al. 2023a, b).  $\text{NO}_3^-$  can cause eutrophication in surface waters and is also relevant in terms of drinking water quality (Katz et al. 2009). During rainfall events, the highly mobile  $\text{NO}_3^-$  enters karst aquifers quickly and can thereby either be diluted (in case of diffuse infiltration) or mobilized (e.g., point infiltration or after fertilization) (Hem 1985; Huebsch et al. 2014). Gadolinium (Gd) belongs to the rare earth elements (REE) (for further information on REE please refer to McLennan 2001, LaMoreaux 2019, and Aide and Nakajima 2020) and is used, e.g., in (high-tech) industry and medical treatments, e.g., magnetic resonance imaging (MRI) contrasting agents (Ebrahimi and Barbieri 2019; Leal Filho et al. 2023; Iyad et al. 2023). Gd is only partially withheld in wastewater treatment plants (WWTP) and thus can serve as a tracer for

wastewater effluents (Knappe et al. 2005; Ebrahimi and Barbieri 2019). Anomalies in the ubiquitously occurring REE can reveal additional (e.g. anthropogenic) input pathways during the underground passage (Bau and Dulski 1996). *Escherichia coli* (*E. coli*) serve as fecal indicator bacteria in water, whereas some strains of *E. coli* are pathogenic and can cause, e.g., gastro-intestinal diseases, urinal infections, and sepsis (Jang et al. 2017; Mohaghegh Motlagh and Yang 2019). Sediment particles can serve as vectors for contaminants (e.g., heavy metals, bacteria, and viruses) (Mahler et al. 2000; Huang et al. 2020) and can cause two types of turbidity in karst systems: (1) Autochthonous (aquifer derived) turbidity is caused by a remobilization of previously deposited sediments in the conduit system, (2) allochthonous (surface derived) turbidity originates from the land surface and is often associated with high levels of total organic carbon (TOC), small sediment particle sizes (0.9–10  $\mu\text{m}$ ), and microbial contamination (Vesper and White 2004; Pronk et al. 2007; Cholet et al. 2019).

The objectives of this study are to (1) Identify possible seasonal changes in the water quality at the Blautopf Spring (karst spring) and in its catchment, including distinct anomalies, (2) better understand small-scale temporal dynamics of the water quality (3) transfer, for the first time, the paired-catchment approach to a subsurface karst conduit system to investigate spatially resolved differences in water quality between different branches of the drainage network (4) identify key parameters of contamination and to assign them to specific land use types to propose measures to improve water quality.

## Material and methods

### Geographical setting and geology

The research site is located on the southern margin of the Swabian-Franconian Jura Mountains, Germany's largest karst landscape and aquifer system. In the area, the Upper Jurassic limestone and marl series exhibits a total thickness of 400 m, providing a significant water storage capacity. The catchment is 165  $\text{km}^2$  large and is well outlined by several tracer tests (Selg and Schwarz 2009; Lauber et al. 2014) (Fig. 1). There are no surface streams on the highly karstified landscape, where sinkholes and dolines allow direct infiltration of precipitation into the karst aquifer.

### Climatic conditions

The catchment is located in a temperate climate with a mean annual average air temperature of 7.0  $^{\circ}\text{C}$  and a mean annual precipitation of 950 mm. Precipitation for the catchment was estimated with a Thiessen polygon method as described in

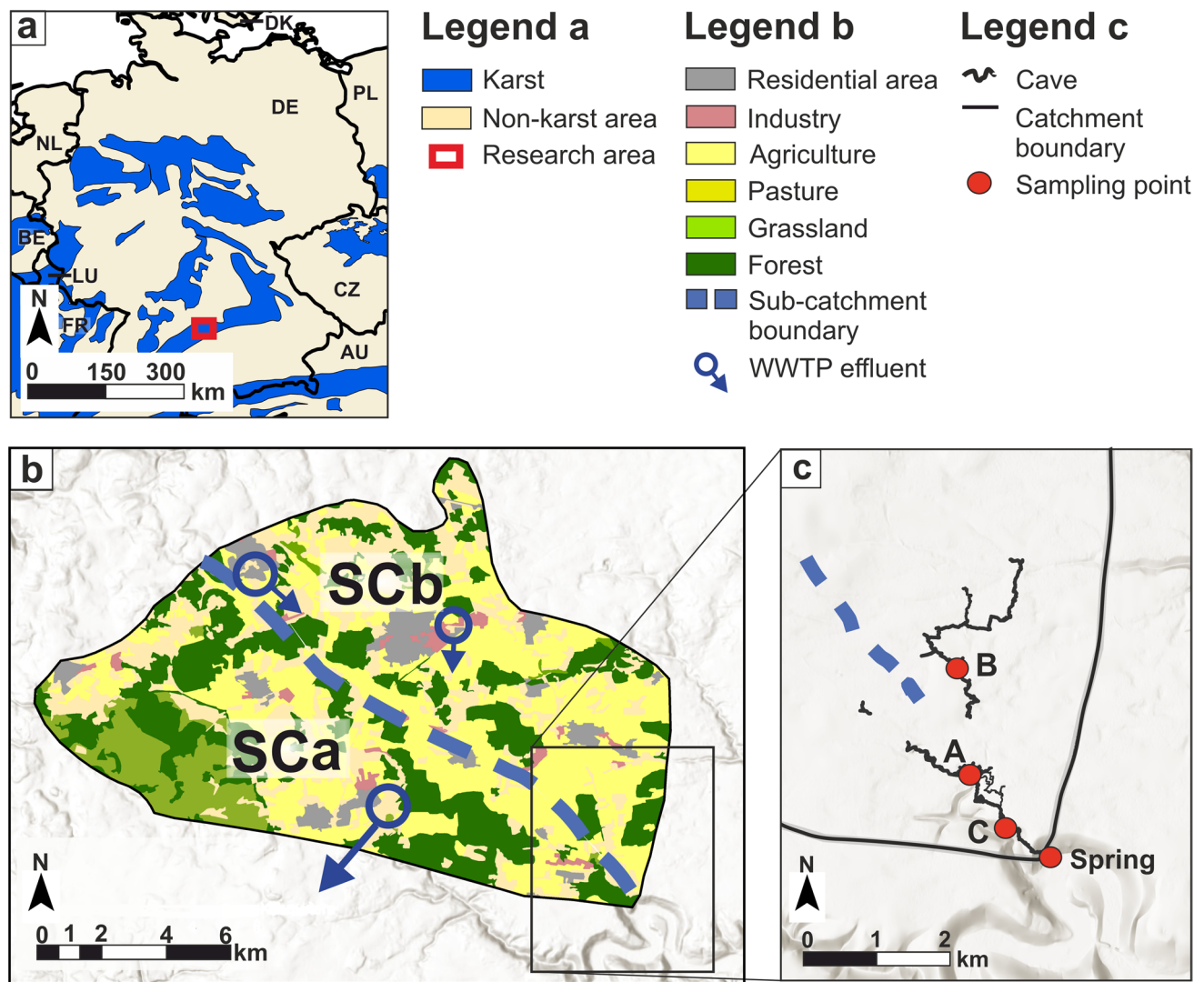


**Fig. 1** a) Location of the catchment shown on a karst map of Europe modified from Chen et al. (2017). b) Land use of the Blautopf catchment area for the sub-catchments *SCa* and *SCb*, including the catchment divide between *SCa* and *SCb*, according to Lauber et al. (2014). Blue circles mark WWTPs, whereas arrows indicate the location of

discharge (inside/outside of catchment area). c) Outlines and locations of the caves in the catchment, with sampling points (A–C) marked in red. Maps were plotted with ArcGIS (Esri), land use in the catchment originates from Corine Land Cover, and cave locations were derived from ARGE Blautopf and ARGE Blaukarst.

Fan et al. (2023). On average, 14% of precipitation consists of snow. Approximately one third of the annual precipitation recharges the aquifer, whereas two thirds are evapotranspiration (Fan et al. 2023).

### Spring hydrology

Blautopf Spring is the only spring that drains this catchment area and is Germany's second largest karst spring. The mean discharge recorded since 1952 is 2300 L/s, with a minimal and maximum discharge of 250 and 32,600 L/s, respectively (Fan et al. 2023, Selg und Schwarz 2009). Discharge measurements are continuously recorded in 15 min

intervals by the Baden-Württemberg state environmental agency (LUBW), the precision of the measurement is within 9% deviation from the mean values. Discharge reacts to precipitation with a lag of around 3 days (Fan et al. 2023). The spring was used for drinking water supply, which was terminated after a noticeable impact on water quality due to wastewater effluents and agricultural runoff in the catchment (Lauber et al. 2014).

### Speleology and active conduit network

The well-developed karst aquifer has an extensive cave system with large conduits. On the basis of speleological

observations, flow measurements and tracer tests, it was possible to show that the catchment can be divided into two sub-catchments, corresponding to two parts of the cave system, both attributing about 50% of water to the spring discharge (Lauber et al. 2014).

Blue Cave with a total current length of 18.1 km (ARGE Blautopf 2024) is located in the Southern sub-catchment (Fig. 1). The cave system provides access to cave streams at several locations. Previous tracer tests showed (Lauber et al. 2014) that the sampling point in the front part of the cave (point C in Fig. 1c) contains water from all currently accessible caves. The rear cave streams (point A) in the Blue Cave, however, only contains water from sub-catchment a (SCa). Both locations were sampled for this study.

The second cave (Hessenhau Cave) with a total length of 8.4 km (ARGE Blaukarst 2014) is located in the northern part of the catchment (SCb, Fig. 1) and in direct connection to one of the WWTPs in the catchment (Lauber et al. 2014). There is one major cave stream with smaller confluences (point B), gathering water from the northern part of the catchment (SCb) and draining into Blue Cave.

Discharge measurements in the caves are very elaborate and were performed with the salt-dilution method (Rantz 1982). For SCa 1500 g and for SCb 2000 g of table salt were injected as Dirac (instantaneous) input and conductivity was measured with two conductivity probes (Multi 3430, WTW) to ensure reliability.

## Land use in catchment

Land use in the catchment consists mainly of agriculture, including animal breeding and pasture (59%), forest and grassland (34%), as well as residential areas and industry (7%) (Fig. 1). There are three WWTPs located in the catchment, whereas two are known to release treated wastewater into the catchment and one drains the water outside of the catchment.

Maps were produced using ArcGIS 10.8.2 (Esri, Inc.) with land use maps obtained from the European Union's Copernicus Land Monitoring Service Information. The spring catchment is based on Selg and Schwarz (2009), sub-catchments (SC) were subdivided according to Lauber et al. (2014) with cave locations from ARGE Blautopf (2020) and ARGE Blaukarst (2014).

## Hydrochemical parameters

### Long-term monitoring at the spring

Water quality monitoring was performed at the spring for a duration of 30 months, from January 2021 until June 2023. This included both water samples and continuous measurements collected at 15 min intervals for hydrochemical

parameters (further described below). Water samples were collected in regular intervals of 1 month, regardless of the hydrological situation, to obtain an overview of the annual changes in hydrochemistry.

### Event sampling

A large precipitation event was monitored to investigate detailed responses of the spring. Event sampling took place from 28 August 2021 to 15 September 2021, for a total duration of 19 days.

For event samples, an auto sampler (Teledyne, ISCO) was installed at the spring to allow for short sampling intervals (2–8 h). Samples in the auto sampler were cooled and single use bags (ProPak, ISCO) were used to collect water samples and to avoid cross contamination.

### Water sampling in caves

In total, 11 cave trips took place between August 2021 and April 2023. Sampling locations (Fig. 1) included the rear part of the Blue Cave (point A), containing water exclusively derived from sub-catchment SCa, a cave lake in the front part of the Blue Cave (point C) containing water from both sub-catchments and Hessenhau Cave (point B) containing water exclusively derived from sub-catchment SCb. The first sampling campaign where both caves were sampled at the same time took place on 12 March 2022, the second sampling campaign on 22 and 23 April 2023. A water sample from the nearby WWTP was collected during one of the sampling campaigns.

Water samples in the cave were taken in chemically inert 1 L bottles (Nalgene, Thermo Scientific). Sample preparation took place in the laboratory within 24 h as described below.

### In situ parameters

In situ parameters were measured in 15-min intervals for 30 months in total at the spring. Temperature, EC, pH, and redox potential were measured with a multiparameter probe (HI9829-03102, Hanna instruments) at a water depth of 1.5 m and cross-checked on a monthly basis by manual measurements with a portable multi-parameter meter (Multi 3430, WTW). In addition to brief on-site calibrations, the continuously installed multiparameter probe was thoroughly calibrated in the laboratory at least once a year. Turbidity was measured with a field-fluorimeter (GGUN FL 30, Albillia).

For event sampling, a particle counter (PCSS fluid lite, Klotz GmbH) was installed at the spring. The device measures all particles in a water volume of 10 mL, for better visualization, results are given in particles per 1 mL



of water. Particles with diameters between 1 and 25  $\mu\text{m}$  were measured. The individual particle sizes classes also include particles that have larger diameters up to the next larger size class, e.g., the size class of 1  $\mu\text{m}$  sums up all particles in the size range of 1–1.9  $\mu\text{m}$  diameter. The sampling interval was set to 5 min, whereas the instrument was automatically rinsed with 40 mL of water prior to each measurement. For continuous sampling at the spring, a 11.8 m long bypass was installed (diameter of 12.7 mm, Rehau Industries) and connected to the particle counter, which operated under a natural gradient. The material of the tube is suitable for drinking water supply (according to German DVGW W270/KTW A) and sufficiently opaque to avoid algae growth and biofilm formation. During the cave trips, in situ parameters (pH, redox potential, EC, temperature) were measured at the respective sampling locations with a multiparameter portable meter (Multi 3430, WTW).

### Sample preparation on site

Samples for TOC measurements were stored in 50 mL brown-glass bottles. TOC samples were acidified with 250 mL hydrochloric acid (37%; Roth Chemicals). Cation and REE samples were filtered with a cellulose acetate filter (0.45  $\mu\text{m}$  pore size, Sartorius AG) on site, stored in 15 mL centrifuge tubes and acidified with 50  $\mu\text{L}$  of concentrated nitric acid (Roth Chemicals). Anion samples were filtered with 0.45  $\mu\text{m}$  cellulose acetate filters without acidification. Measurement for bicarbonate ( $\text{HCO}_3^-$ ) were done on site as triplicates with an alkalinity test (MColortest, Merck KGaA).

### Laboratory measurements

In the laboratory, anion samples were diluted and measured with ion-chromatography (IC 2100, Dionex). Major cations, trace elements, and REE were measured with inductively coupled plasma mass spectrometry (ICP-MS 7800, Agilent technologies). During ICP-MS measurements, internal standards (ICP-MS calibration standard 1 and 2 in 2%  $\text{HNO}_3$  (VWR) and MULTI-ELEMENT ICP standard solution ROTISTar 4 elements in 2%  $\text{HNO}_3$ , concentration of 1 mg/L (Carl Roth)) were used. A drift control for each measurement series was performed with a 5  $\mu\text{g/L}$  internal standard (see above). TOC samples were measured in triplicates with a vario TOC cube (Elementar). Samples for the analysis of coliforms and *E. coli* were diluted 4- to 25-fold (in particular event samples) with bi-distilled water, based on results from the previous day. After an incubation time of 24 h at 35  $^\circ\text{C}$ , results from the rapid test (IDEXX Laboratories, Inc.) are reported as the most

probable number (MPN) per 100 mL. Samples exceeding the maximum capacity of 2419 MPN/100 mL are presented in red. MPN is a statistical number of bacteria colonies (with a 95% confidence interval) that would form if the sample was grown on a plate or petri dish. Results from plate counts are commonly measured in colony forming units (CFU), whereas 1 MPN statistically approximates 1 CFU (Cho et al. 2010; IDEXX 2025).

### Statistical analysis and data evaluation

To investigate seasonal behavior of selected parameters, samples were separated on the basis of calendrical seasons. Data for long-term monitoring and event sampling were plotted and analyzed with the software Origin Pro (OriginLab), using a pairwise Spearman rank correlation after testing for normal distribution with a Kolmogorov–Smirnow test. Significance level of correlations were 95% ( $p = 0.05$ ) and only strong positive ( $>0.6$ ) or strong negative ( $\leq 0.6$ ) correlations were interpreted.

REE data were normalized to PAAS (Post Archean Australian Shales) (McLennan 2001). For the calculation of Gd anomalies, an interpolation of expected PAAS normalized concentrations (indicated by \*) of neighboring elements was used (Bau and Dulski 1996):

$$\text{Gd}_{\text{PAAS}}/\text{Gd}_{\text{PAAS}^*} = \frac{\text{Gd}_{\text{PAAS}}}{0.33 \times \text{Sm}_{\text{PAAS}} + 0.67 \times \text{Tb}_{\text{PAAS}}} \quad (1)$$

with PAAS normalized values of the REEs Gd ( $\text{Gd}_{\text{PAAS}}$ ), samarium ( $\text{Sm}_{\text{PAAS}}$ ), terbium ( $\text{Tb}_{\text{PAAS}}$ ), and expected PAAS normalized Gd values ( $\text{Gd}_{\text{PAAS}^*}$ ).

The residence time of percolated precipitation water in the aquifer was estimated by performing a cross-correlation (OriginLab 2021) that is used to establish a link between input time series and output times series. The cross-correlation function  $r_{xy}(k)$  is described as (Larocque et al. 1998):

$$r_{xy}(k) = \frac{C_{xy}(k)}{\sigma_x \sigma_y} \quad (2)$$

$$C_{xy}(k) = \frac{1}{n} \sum_{t=1}^{n-k} (x_t - \bar{x})(y_{t+k} - \bar{y}) \quad (3)$$

with the input series  $x$  and output series  $y$ , the time lag  $k$ , the cross-correlogram  $C_{xy}(k)$ , and the standard deviation  $\sigma$  and time  $t$ .

Some data are shown in the form of a heat map to facilitate a general overview. Concentrations of data points for each compound were divided by the maximum concentration ( $c/c_{\text{max}}$ ), and colors therefore describe a relative concentration in comparison to the highest measured concentration of the respective compound.

## Results and discussion

### Seasonal variations of water quality

Spring discharge varied between 0.1 and 23.1 m<sup>3</sup>/s, with a mean of 1.71 m<sup>3</sup>/s during the monitoring period of 30 months (Fig. 2). Water temperature varied between 9.2 and 10.5 °C, variations between day and night reached up to  $\pm 0.3$  °C due to sun radiation in the upper water column, which was not observed in the cave system with an annual water temperature of  $9.6 \pm 0.2$  °C.

Median values were for pH 7.17, EC 654  $\mu$ S/cm, redox potential +398 mV, and turbidity 3.56 FNU (Table 1). The highest values for precipitation (64.5 mm/day), discharge (23.1 m<sup>3</sup>/s), and turbidity (2132 formazin nephelometric units (FNU)) were observed during a heavy rainfall event in July 2021. All parameters had returned to baseline conditions after the major rainfall event in July 2021. In situ parameters that were measured during a monitored rainfall event in August and September 2021 are also presented in Table 1 for a better categorization into the behavior of the spring.

Major ions, trace elements and REE show variable behavior during long-term monitoring (Fig. 2). Most parameters

show strong variations over the course of the year, whereas  $\text{HCO}_3^-$ ,  $\text{Ca}^{2+}$ ,  $\text{Mg}^{2+}$ , V, Sr, U, and Ba only show minimal changes. Selected parameters (EC,  $\text{NO}_3^-$ ,  $\text{Cl}^-$ ,  $\text{K}^+$ , Gd, and *E. coli*) were chosen on the basis of the relevance to the land use in the catchment and are described in more detail in the sections below, values for these parameters are given in Table 2. Concentrations were always below the thresholds for drinking water, e.g., according to the European Water Framework Directive (European Union 2020), with the exception of *E. coli*.

### Chloride

$\text{Cl}^-$  featured the highest concentrations in winter but also showed high variability in fall and spring, with lower concentrations during summer (Fig. 2 and 3).

This is likely influenced by road salt which is applied during snowy conditions throughout the catchment, which can occur from fall to spring, and is flushed into the karst aquifer during snowmelt events (Baraza and Hasenmueller 2021).

In the long-term monitoring data,  $\text{Cl}^-$  showed a strong positive correlation with  $\text{SO}_4^{2-}$ ,  $\text{Na}^+$ ,  $\text{K}^+$ , Rb, Sr, and Cs (Fig. 4), only significant ( $>0.6$ ,  $p = 0.05$ ) correlations were considered. In particular, the positive correlation

**Fig. 2** Precipitation and discharge from long-term monitoring at Blautopf Spring, including sampling dates (red triangles). Below a heat map of selected parameters, normalized to maximum values, ( $c/c_{\text{max}}$ ), whereas light (yellow) colors indicate maximum values and dark (magenta) colors indicate minimum values. Color bars on the bottom indicate the respective annual (calendrical) seasons. Missing values and measurements below the limit of detection (LOD) are left blank.

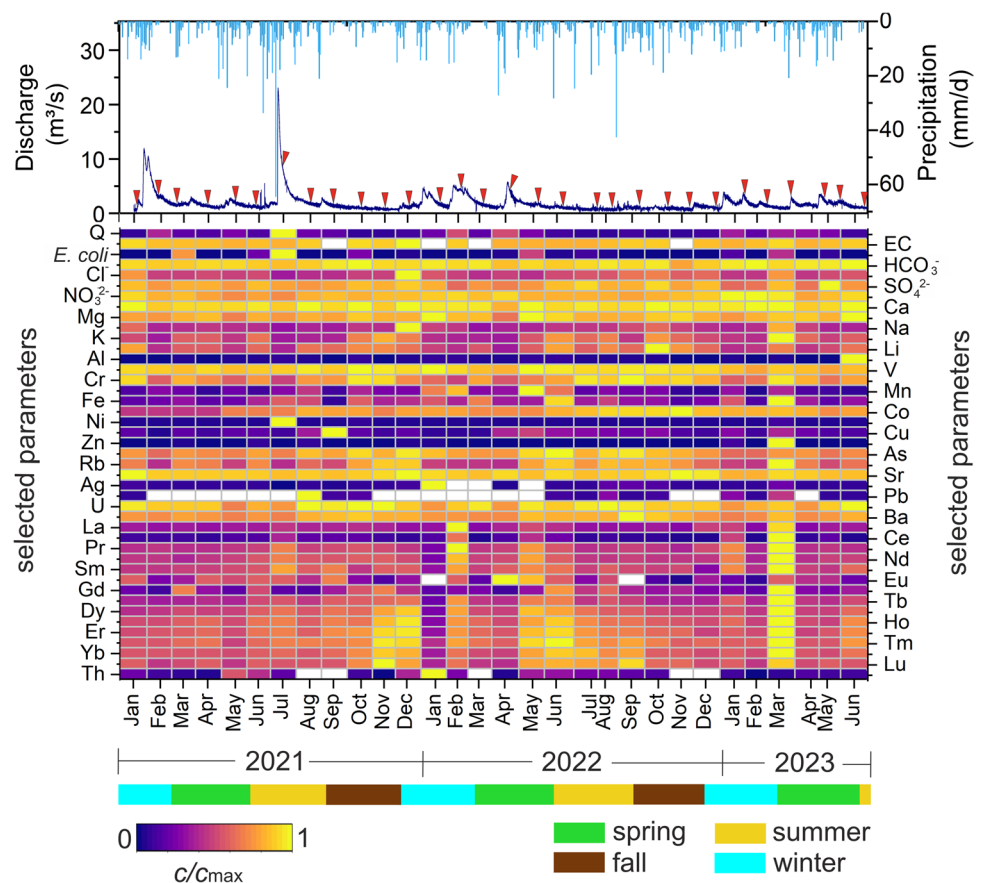


**Table 1** In situ parameters, discharge, and precipitation measured at the spring during the 30-months monitoring period (January 2021 to June 2023), and during the rainfall event in August/September 2021

Parameter	Unit	Long-term monitoring (30 months)				Rainfall event		
		Median	Mean	Min	Max	Mean	Min	Max
Precipitation	mm/day	0.3	2.4	0	64.5	0.1	0	3.6
Discharge	m <sup>3</sup> /s	1.3	1.7	0.1	23.1	1.7	1.1	2.7
Temperature	°C	9.49	9.51	9.18	10.50	9.54	9.48	9.77
pH	-	7.25	7.17	5.88	8.07	7.16	7.09	7.23
EC	μS/cm	654	655	520	1063	674	634	698
Redox potential	mV	398	382	161	465	419	381	444
Turbidity	FNU	3.56	15.47	1.18	2132	0.16	0.09	0.29

**Table 2** Selected parameters for long-term monthly monitoring, rainfall event samples, and cave grab samples

Parameter	Unit	Statistic	Long-term monitoring (30-month)					Rainfall event	Cave samples			
			Total	Winter	Spring	Summer	Fall		Total	SCa	SCb	C lake
NO <sub>3</sub> <sup>-</sup>	mg/L	mean	26.4	28.1	26.3	25.3	25.7	25.4	23.1	30.0	26.2	25.7
		min	22.0	25.1	22.7	22.0	24.4	21.1	16.3	27.5	21.8	21.5
		max	31.2	31.2	30.1	28.4	26.4	30.0	28.7	32.6	30.2	31.2
		median	26.3	27.9	26.1	25.3	25.8	25.5	23.2	29.9	25.8	26.0
Cl <sup>-</sup>	mg/L	mean	28.6	31.9	27.4	26.3	29.5	22.9	18.8	29.4	24.7	23.9
		min	19.6	24.1	23.0	19.6	22.2	20.1	17.3	24.6	23.1	21.2
		max	53.5	53.5	39.6	29.6	26.0	31.9	23.4	33.3	26.6	27.4
		median	26.7	27.7	25.8	27.9	29.0	22.4	17.9	30.2	24.5	23.4
K <sup>+</sup>	mg/L	mean	1.46	1.27	1.50	1.53	1.65	1.34	0.79	1.58	1.42	1.38
		min	0.93	0.97	0.97	0.93	1.06	0.92	0.60	1.15	1.01	1.01
		max	2.68	1.85	2.68	1.97	2.21	2.40	0.95	2.01	2.24	2.45
		median	1.42	1.15	1.46	1.65	1.63	1.31	0.78	1.58	1.28	1.28
Gd	ng/L	mean	12.0	7.6	13.8	13.9	14.2	10.7	2.4	16.1	9.4	10.9
		min	3.7	3.7	3.9	5.0	9.9	5.1	0.7	9.7	3.4	5.6
		max	31.9	12.9	31.9	23.6	21.4	28.2	3.4	20.9	24.1	27.7
		median	10.5	7.6	10.5	14.9	12.3	8.8	2.7	16.8	7.2	9.5
<i>E. coli</i>	MPN/100 mL	mean	693	131	1538	1064	277	2340	59	142	104	120
		min	4	4	21	4	38	38	2	4	2	4
		max	5199	744	3973	5199	1298	17,168	180	395	325	437
		median	101	11	1255	258	88	281	41	84	60	80
Total coliforms	MPN/100 mL	mean	1372	243	2959	2064	707	5463	183	2983	337	1323
		min	11	11	163	17	156	226	4	22	8	17
		max	7945	1164	6499	7945	2407	30,082	626	8664	1102	9135
		median	431	34	2818	1633	309	1642	89	689	231	312
Total number of samples			30	8	8	8	6	149	6	5	6	9

between Cl<sup>-</sup> and Na<sup>+</sup> supports the assumption that high winter Cl<sup>-</sup> is derived from road salt, which also influences the continuously measured EC, that was usually low during high discharge conditions in summer and higher during high discharge conditions in the winter months (Jan–Mar). Typically, the EC of spring water decreases when large quantities of freshly infiltrated water arrive

at the spring (White 2015), which occurs during rainfall, whereas snowmelt water often contains high concentrations of sodium chloride (NaCl) from road salt. Similar observations of Cl<sup>-</sup> input from road salt have been reported for Blautopf and other karst springs as well (Selg and Schwarz 2009; Perera et al. 2010; Baraza and Hasenmueller 2021; Overbo et al. 2021).

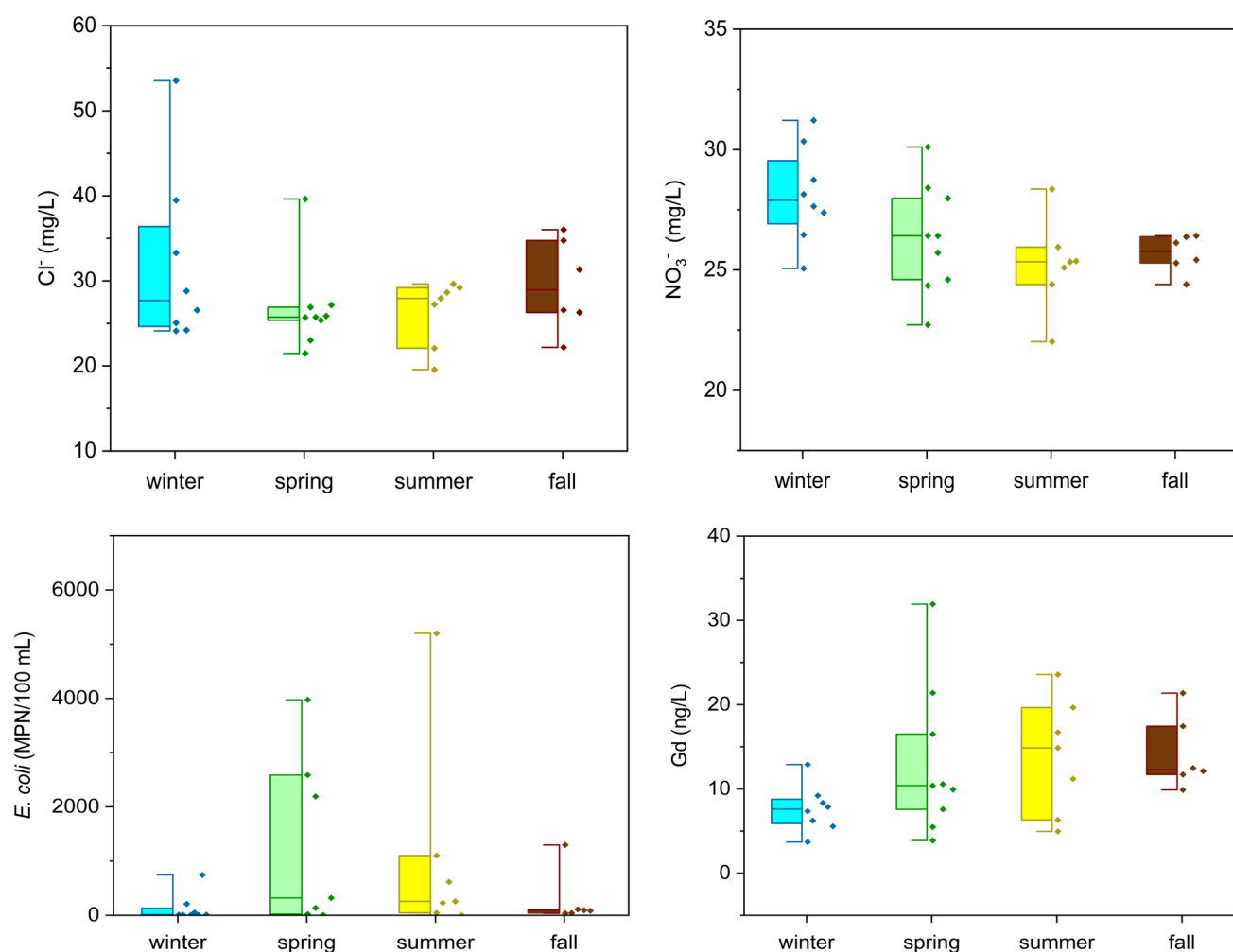


**Fig. 3** Box and whisker plot diagrams for long-term monitoring samples at the spring in monthly intervals, distributed after the respective annual seasons for  $\text{Cl}^-$ ,  $\text{NO}_3^-$ , *E. coli* bacteria, and Gd. For each sea-

son, box and whisker plots on the left show median, minimum, and maximum values as well as quartiles. Dots on the right of each box and whisker depict measured values.

### Nitrate

$\text{NO}_3^-$  showed the highest concentrations in winter with gradually decreasing concentrations during the rest of the hydrological year (Fig. 3).

These annual changes can likely be related to fertilizing of crops, where excess  $\text{NO}_3^-$  is flushed into the underlining karst aquifer (Strebel et al. 1989; Yue et al. 2019; Wang et al. 2020) and often stored in the epikarst (Husic et al. 2019). Concentrations in this study were lowest in summer, when denitrification and increased  $\text{NO}_3^-$  uptake by plants often leads to a decrease in groundwater  $\text{NO}_3^-$  (Huebsch et al. 2014; Yue et al. 2018). In general, mean annual  $\text{NO}_3^-$  concentrations of 26.4 mg/L strongly support an agricultural influence, compared to springs without agricultural influence that exhibited concentrations of around 3.7 mg/L

in other studies (Weber and Kubiniok 2022). Long-term  $\text{NO}_3^-$  monitoring showed a significant strong positive correlation with  $\text{Ca}^{2+}$ . A significant strong negative correlation of  $\text{NO}_3^-$  with other parameters was not found (Fig. 4).

### Gadolinium

The highest concentrations of Gd (13.1–14.2 ng/L) were observed in springtime, summer, and fall, whereas mean values for winter were lowest with a value of 7.6 ng/L (Table 2 and Fig. 3). A significant negative correlation was found with discharge. In contrast, Gd showed a significant positive correlation with  $\text{K}^+$ , Li, Cr, Rb, Ba, Dy, Ho, Er, Tm, Yb, and Lu in the long-term monitoring data (Fig. 4). All samples showed a positive Gd anomaly with a mean of  $\text{Gd}/\text{Gd}^* = 4.6$  and a range of  $\text{Gd}/\text{Gd}^* = 1.9$  to  $\text{Gd}/\text{Gd}^* = 11.2$ .



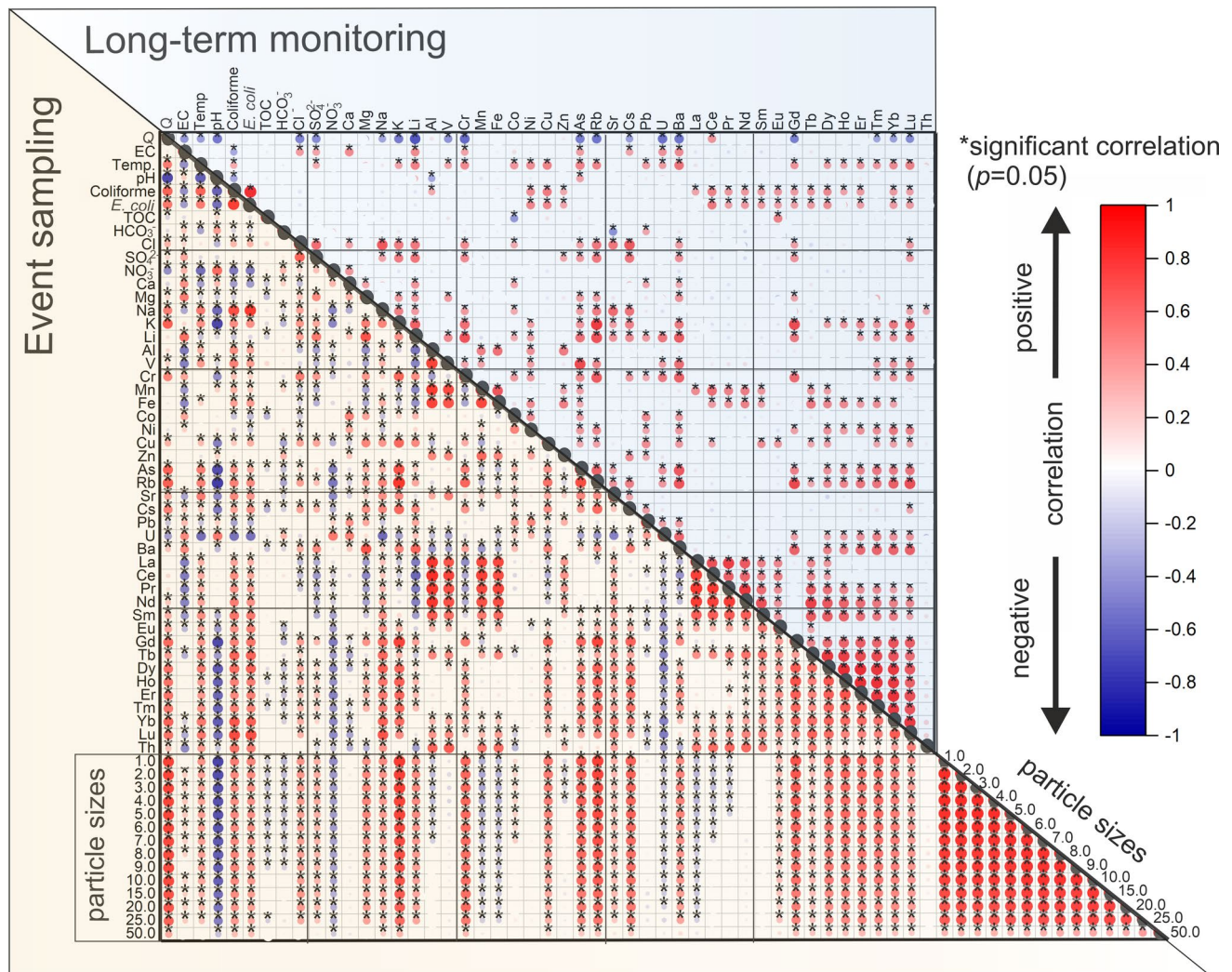


**Fig. 4** Results for a Spearman rank correlation test for long-term monitoring data (upper triangle in blue) and event samples (lower triangle in orange). Red dots indicate a positive correlation; blue dots indicate a negative correlation; only significant correlations are shown.

Gd concentrations showed high variability due to hydrological and anthropogenic factors. Dilution was identified as a dominant factor influencing the behavior of Gd in the long-term monitoring data. This pattern indicates a continuous input of Gd, which is diluted with increasing discharge, often after rainfall events. A positive Gd anomaly describes above average concentrations of Gd in comparison to other REEs when standardized to PAAS. These excess Gd loads are often related to an anthropogenic influence (Bau and Dulski 1996). WWTPs are a typical recipient of anthropogenic Gd, as hospital patients receiving MRI scans excrete Gd following their return home, which can be responsible for weekly Gd variations (Nödler et al. 2011; Brünjes et al. 2016; Boester and Rude 2020). A possible origin from a WWTP

is further supported by the positive correlation with Li and Rb, which are also associated with WWTP effluents (Choubert et al. 2011).

#### Potassium

A gradual increase of potassium ( $K^+$ ) in the course of the year was observed from winter to fall (data not shown), showing a similar behavior to Gd. In addition,  $K^+$  also showed a significant negative correlation with discharge (Fig. 4). In the long-term monitoring data,  $K^+$  showed a significant positive correlation with  $Cl^-$ ,  $SO_4^{2-}$ , Mg, Li, Cr, As, Rb, Ba, Gd, Yb, and Lu.

A negative correlation of  $K^+$  with discharge can be explained by a dilution effect with a relatively constant  $K^+$

input. This also means that decreasing discharge over the course of the year leads to increasing  $K^+$  concentrations. Apart from a geogenic origin of  $K^+$  (Hem et al. 1985), there are likely other anthropogenic sources contributing to  $K^+$  concentrations at the spring. Gd and Rb have been associated with wastewater effluents (Bau and Dulski 1996; Choubert et al. 2011) and  $K^+$  is a major constituent in mineral fertilizer, which is often applied in agricultural areas and leaches from the soil into karst aquifers (Perrin et al. 2003; Wu et al. 2025).

### Fecal bacteria

Fecal bacteria (total coliforms and *E. coli*) were detected in all monthly samples throughout the year with concentrations ranging from 11–7945 MPN/100 mL (total coliforms) and 1–5199 MPN/100 mL (*E. coli*). During long-term monitoring, coliforms and *E. coli* showed a strong positive correlation. *E. coli* further showed a significant strong positive correlation with Ni, Cu, and Ce. A significant strong negative correlation could not be detected in the long-term monitoring data (Fig. 4). Seasonal variations show highest concentrations during springtime and summer (Table 2 and Fig. 3).

The omnipresence of *E. coli* underlines a continuous but highly variable input of fecal bacteria into the aquifer during all seasons and flow conditions, with a predominance during springtime and summer. Possible sources could be both settlements and agriculture, including the herding of animals in the catchment area (Katz et al. 2009; Kelly et al. 2009; Knierim et al. 2015). Monthly measurements only provide a coarse temporal overview but nevertheless display a high variability of fecal bacteria at this karst spring.

It is important to note that the correlation analysis of the long-term monitoring data is only partially conclusive, as samples were only taken at one day each month, at different weekdays and at different hydrological situations, this might result in weaker correlations for individual parameters.

### Event-based monitoring

During the rainfall event (28 August 2021 to 15 September 2021) with a total precipitation of 55.3 mm occurring over 4 days, the discharge increased from 1.5 m<sup>3</sup>/s ( $\pm 0.1$  m<sup>3</sup>/s) before the event to a maximum of 2.7 m<sup>3</sup>/s and then returned to pre-event conditions within 8 days (Fig. 5). Concentrations for selected parameters are given in Table 1 and 2.

A strong positive correlation between discharge and temperature, coliforms, *E. coli*, Na,  $K^+$ , As, Rb, Cs, Gd, Dy, Ho, Er, Tm, Yb, Lu, and all particle sizes could be detected (Fig. 4). A strong negative correlation of discharge was found with pH and  $NO_3^-$  (Fig. 4). Further significant, but weaker ( $<0.6$ ) correlations can be seen in Fig. 4. Most

parameters show similar behavior (Figs. 5 and 6), whereas selected parameters are discussed in more detail below.

A positive correlation with discharge indicates an overall mobilization of compounds during the rainfall event and subsequent transport through the aquifer (Vesper et al. 2001). A change of temperature and pH is an indicator for changing hydrological conditions and the arrival of freshly infiltrated precipitation, indicating shorter groundwater residence times with less time for equilibration with the surrounding limestone. However, pH in karst aquifers is influenced by a range of processes, mainly carbonate dissolution, but also temperature,  $CO_2$  partial pressure and microbial activity, and therefore needs to be interpreted with care (Pu et al. 2014; Luo et al. 2023). A significant negative correlation between discharge and  $NO_3^-$  was detected as well, pointing toward dilution during the rainfall event (as described in more detail below).

Approximately 2–3 days after the start of the rainfall event, discharge started to rise (T1) with a simultaneous increase of particle counts (1  $\mu$ m and 10  $\mu$ m are shown in Fig. 5). This well-defined peak contained three minor peaks. Both turbidity and particle counts decreased again thereafter, whereas all other measured parameters did not show any change at this stage. This is considered an autochthonous response of the system, where water and sediment particles, previously stored in the cave system and epikarst, are pushed out of the system. A pressure pulse leads to an increase in flow velocity and turbulence, resulting in increased particle counts at the spring during the rising limb of spring discharge hydrograph. Particles detected during the first peak (T1) are interpreted to have been previously present within the cave system and are remobilized during this phase (Aquilina et al. 2006; Pronk et al. 2007, 2009).

The increase of water temperature as well as a decrease in  $NO_3^-$ ,  $Ca^{2+}$  and  $HCO_3^-$  (T2) mark the arrival of freshly infiltrated rainwater and therefore the beginning of the allochthonous phase. Simultaneously, *E. coli*,  $K^+$ ,  $Cl^-$ , Gd and all particle counts increase. The particles measured at this stage are considered to originate from the land surface and were flushed into the aquifer through fractures and conduits (Williams 1983; Perrin et al. 2003; Pronk et al. 2007, 2009). Discharge gradually starts to decrease during this phase. EC remains constant, which is interpreted to reflect the combination of mobilized and diluted parameters, which results in an overall absent EC response to the rainfall event. While some ions decrease (e.g.,  $NO_3^-$ ,  $Ca^{2+}$ , or  $HCO_3^-$ ), others increase (e.g., Gd,  $K^+$ , or  $Cl^-$ ), and so the total ion concentration in the water initially remains largely unchanged, although individual ions begin to show changes (T2, Fig. 5). The change in hydrological conditions is also reflected by changes in water temperature and pH (data not shown).

EC only started to decrease right after all mobilized parameters (with the exception of 10  $\mu$ m particles) reached their maximum concentration (T3). The lowest values of

EC coincide with the minimum values of diluted parameters (e.g.,  $\text{Ca}^{2+}$ ,  $\text{NO}_3^-$ ), marking the highest dilution by freshly infiltrated precipitation (e.g., White 2015). A gradual return to baseline conditions for all previously mobilized parameters then occurs (T4). Small peaks in water temperature are caused by sunny days, which warm the upper part of the water column of the spring. Discharge shows a slow recession (T4), indicating a significant proportion of slow infiltration in the unsaturated zone (Pinault et al. 2001).

The strength of increase or decrease of individual parameters is further given in Fig. 6.

When considering the rainfall as an input function of surface-derived parameters, their change in concentration can serve as an estimation for the residence time of percolated precipitation water in the aquifer (Pinault et al. 2001; Mahler and Garner 2009; Doummar et al. 2014). The time lag calculated by cross-correlation between rainfall and diluted parameters (e.g.,  $\text{HCO}_3^-$ ,  $\text{NO}_3^-$ ) was 100 h and for mobilized parameters (e.g., Gd and  $\text{Cl}^-$ ) 74–78 h. The time lag for discharge was calculated to be 60 h for the investigated rainfall event.

The rate at which the discharge of a karst spring reacts to a rainfall event is primarily related to the intensity of the rainfall event, with more intensive rainfall events often triggering faster responses. The overall precipitation volume conversely distinguishes the strength of the reaction (Tobin et al. 2021). The observed lag time of 60 h for discharge is faster than the calculated average lag time of 3 days for the response of discharge to daily precipitation at Blautopf Spring (Fan et al. 2023). This comparatively fast and strong reaction of the discharge underlines that the observed rainfall event was both intense and involved a relatively high amount of precipitation. However, discharge in karst aquifers comprises primarily groundwater baseflow and water from the epikarst but only up to 30% of freshly infiltrated precipitation (Perrin et al. 2003; Pronk et al. 2009; Tobin et al. 2021), in some cases up to 55% (Mahler and Garner 2009).

The epikarst acts as an intermediate reservoir and can provide significant storage for freshly infiltrated rainwater if sufficiently deep, which replaces water previously stored in the fine-fissured epikarst, leading the excess water to flow through larger conduits. At the same time, precipitation also enters the karst aquifer directly through swallow holes at the land surface. Infiltration of precipitation therefore takes place both through the finer-fissured epikarst and conduits alike, whereas the residence times in conduits are significantly lower (Williams 1983; Perrin et al. 2003; Bakalowicz 2004). Precipitation hence leads to a dilution of parameters with a respective residence time of approximately 100 h. On the other hand, precipitation can also lead to a mobilization of water quality parameters from the land surface, exhibiting a residence time of approx. 74–78 h. Both dilution and mobilization show relatively short residence times, which

are typical for highly developed karst systems (Fan et al. 2023). The resulting hydro- and chemographs are usually a combination of pre-event water (stored, e.g., in the epikarst) and event water and thus cannot always clearly be separated (Pinault et al. 2001; Doummar et al. 2014). As the memory of the aquifer is about 40 days (Fan et al. 2023), the residence times in this rainfall event still mainly comprises fast flow components (Mahler and Garner 2009) but probably still approximates best the mean overall residence time of precipitation water for this event, from percolation until discharge at the spring.

Calculated residence times for diluted and mobilized parameters are similar to mean transit times for conservative tracers of 81–179 h (at spring discharges of 3760 and 1044 L/s, respectively), that were injected at a local WWTP close to the center of the catchment into a highly karstified doline and 155–420 h (at spring discharges of 3140 and 975 L/s, respectively) for a tracer injection at the margin of the catchment, which included a substantial travel time through the unsaturated zone (Villinger and Ufrecht 1989; Lauber et al. 2014).

Spring discharge shows a quicker response if the epikarst is saturated with water in comparison to a rainfall event after dry conditions (Aquilina et al. 2006; Tobin et al. 2021). This could likely be observed for the investigated rainfall event, which succeeded another major rainfall event taking place in July 2021, with spring discharge reaching up to 23.1 m<sup>3</sup>/s (on 09 July 2021). This previous significant flushing of the aquifer might have also influenced contaminant and sediment transport, by adding (input from the land-surface by slow and fast infiltration) and removing (by flushing of pre-event epikarst water) these components from the aquifer (Vesper et al. 2001; Mahler and Massei 2007; Toran and Reisch 2013). Although the overall reaction of karst springs can be similar for rainfall events, the reaction of individual solute and particulate compounds, including viruses and bacteria, often differs (Vesper et al. 2001; Pronk et al. 2009; Flynn and Sinreich 2010; Tobin et al. 2021). Selected parameters are thus discussed in more detail below:

### Chloride

$\text{Cl}^-$  showed an increase in concentration after the rainfall event (Fig. 5). A significant strong positive correlation was found with Cr and weaker positive correlations were found with  $\text{Na}^+$ ,  $\text{K}^+$ , Cr, Cu, Rb, Gd, and all particle sizes.

$\text{Cl}^-$  is highly soluble in water and thus easily transported into karst during rainfall events (Pinault et al. 2001). This natural tracer is, besides its geogenic origin (Jakeman et al. 2016), a major constituent in agricultural activities and wastewater, e.g., from household chemicals and urine (Pinault et al. 2001; Overbo et al. 2021). Peaks of  $\text{Cl}^-$ , and thus a mobilization, in karst aquifers have in particular been



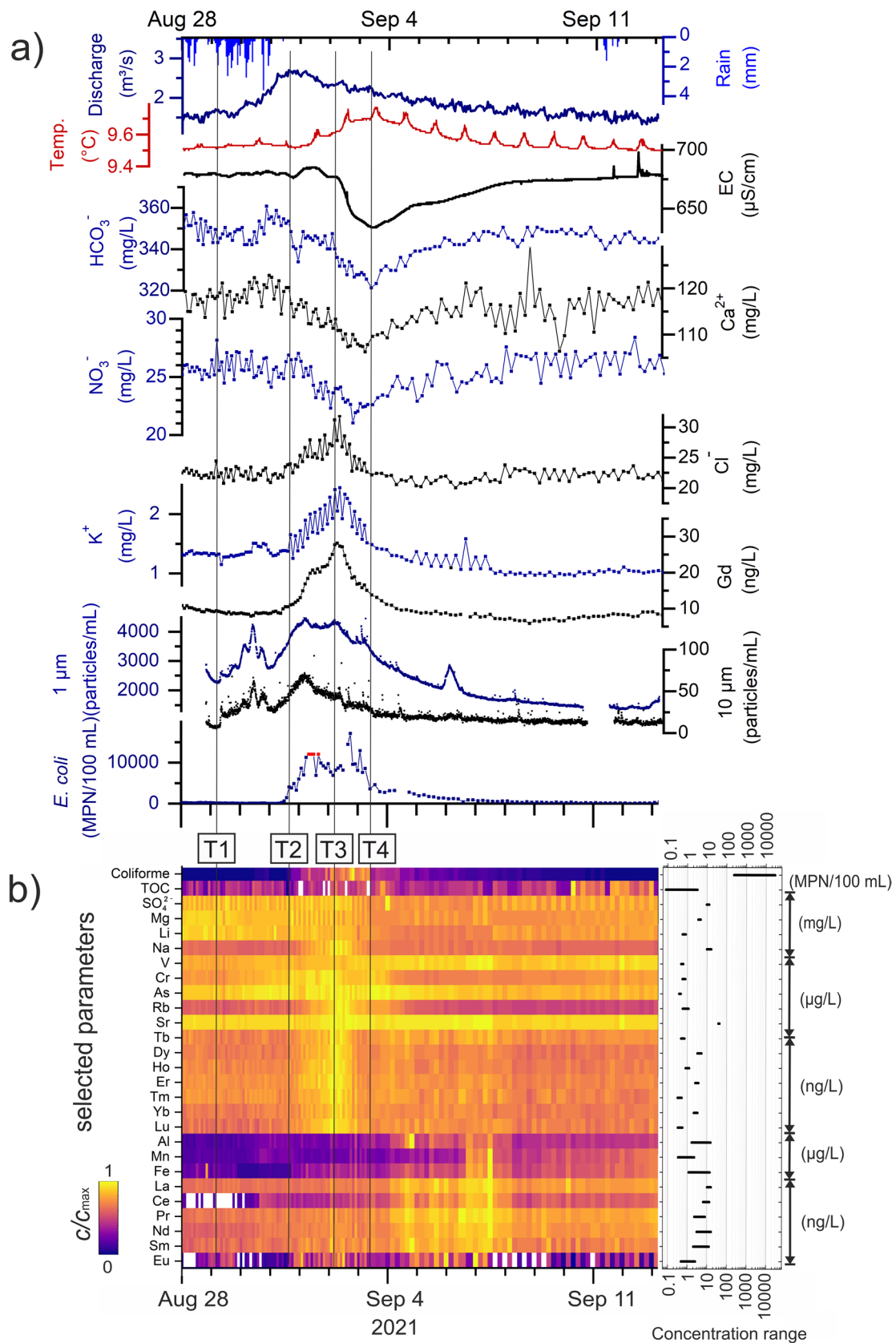


**Fig. 5** **a)** Measured values at the spring for precipitation, discharge, temperature, EC,  $\text{HCO}_3^-$ ,  $\text{Ca}^{2+}$ ,  $\text{NO}_3^-$ ,  $\text{Cl}^-$ ,  $\text{K}^+$ , Gd, 1  $\mu\text{m}$  and 10  $\mu\text{m}$  particle counts, and *E. coli* from event sampling from 27 August until 13 September 2021. Values for *E. coli* bacteria exceeding the test capacity are marked in red. Phases T1–T4 are highlighted. **b)** Selected parameters, normalized to the individual maximal measured value, are shown in the heat map. Bars on the right show the range of log concentrations for each parameter in the given unit

linked to sewer overflows (Heinz 2009). A similar behavior of  $\text{Na}^+$ ,  $\text{K}^+$  and  $\text{Cl}^-$  hints toward an anthropogenic influence (Ender et al. 2017) for this rainfall event and especially Rb is often only partially removed by WWTPs (Choubert et al. 2011). Further sources of  $\text{Cl}^-$  could include the application of manure or KCl mineral fertilizers (Visser et al. 2021); however, in this case a dilution would have been expected during the rainfall event (as described in more detail for  $\text{NO}_3^-$ ). Overall, there are likely several different sources for  $\text{Cl}^-$  in the catchment area that result in a combined signal of  $\text{Cl}^-$  concentrations.

### Nitrate

$\text{NO}_3^-$  concentrations decreased after the rainfall event and showed a significant strong positive correlation with pH, Ca, Pb, and U and a significant strong negative correlation with temperature, coliforms, *E. coli*, As, Rb, Gd, and Er (Fig. 4).

$\text{NO}_3^-$  mainly originated from agricultural activities at the land surface and is highly soluble in rainwater. Therefore, it is easily transported into karst aquifers, where it can be stored in the unsaturated zone, including soil and epikarst but also transported through larger conduits, e.g., in the context of rainfall events (Pinault et al. 2001; Husic et al. 2019). Typical sources of  $\text{NO}_3^-$  include N-containing fertilizers, the application of manure, (industrial) wastewater and soil nitrogen (Smith et al. 2020; Wang et al. 2023; Zhang et al. 2023b). There is no major  $\text{NO}_3^-$  emitting industry in the catchment area.

A simultaneous decrease of  $\text{NO}_3^-$ ,  $\text{Ca}^{2+}$ ,  $\text{HCO}_3^-$ , and later EC (Fig. 5) supported the dilution of  $\text{NO}_3^-$  with freshly infiltrated rainwater (Ryan and Meiman 1996; Pronk et al. 2009).  $\text{NO}_3^-$  in the catchment is applied primarily during springtime and summer, over a large area within the catchment, resulting in a diffuse agricultural input (Fig. 1 and Fig. 3). Conversely, lower  $\text{NO}_3^-$  concentrations in the soil are expected in late summer when the monitored rainfall event took place. In addition, preceding this event another very heavy rainfall event took place, which most likely already transported  $\text{NO}_3^-$  from the land surface into the aquifer and may as well have flushed potentially stored  $\text{NO}_3^-$  from the epikarst (as described above). Hence a decrease in  $\text{NO}_3^-$  concentrations after the monitored rainfall event can be explained as dilution by freshly infiltrated precipitation (Husic et al. 2019). Mahler et al. (2008) made

a similar observation and attributed the origin of  $\text{NO}_3^-$  to continuous leaching of fertilizers and soil nitrogen. Nevertheless, the correlation between  $\text{NO}_3^-$  and discharge is complex and depends strongly on the season (e.g., recent  $\text{NO}_3^-$  application during springtime) as well as previous  $\text{NO}_3^-$  accumulation in the soil and unsaturated zone. Mobilization of  $\text{NO}_3^-$  during a rainfall event would be possible as well (Mahler et al. 2009; Huebsch et al. 2014; Smith et al. 2020; Wang et al. 2022).  $\text{NO}_3^-$  peaks after heavy rainfall events and overall elevated  $\text{NO}_3^-$  concentrations have also been linked to leakage of septic tanks and sewers as well as application of treated wastewater on agricultural fields, which contains low  $\text{NO}_3^-/\text{Cl}^-$  ratios but high ammonium levels (Katz et al. 2009; Caetano Bicalho et al. 2012; Grimmeisen et al. 2017). Especially when event water is transported fast through well-established conduits (e.g., Perrin et al. 2003) possible ammonium from WWTP effluents will only remain in the aquifer for a short period of time and thus not be subject to nitrification (Böhlke 2002; Zhang et al. 2023b). A dilution of  $\text{NO}_3^-$  after the monitored rainfall event therefore does not contradict a sewer overflow. In this study, nitrogen was measured only in the form of  $\text{NO}_3^-$ , but not in other redox states as in, e.g., ammonium. However, in future studies this could help to better distinguish the origin of nitrogen together with measurements of isotopic signatures (Böhlke 2002; Grimmeisen et al. 2017).

Wastewater may therefore contribute to the overall nitrogen load but does not impact  $\text{NO}_3^-$  concentrations during the rainfall event, supported by the strong negative correlation with WWTP effluent associated elements like Gd or Rb (Choubert et al. 2011; Boester and Rüde 2020). The most probable origin for  $\text{NO}_3^-$  in the Blautopf catchment is therefore a continuous but moderate input from agriculture following storage in the epikarst, where  $\text{NO}_3^-$  is diluted by freshly infiltrated rainwater (Mahler et al. 2008; Husic et al. 2019). Although nitrogen is often applied in the form of ammonium on agricultural fields,  $\text{NO}_3^-$  is often the major form of nitrogen in agricultural runoff (Böhlke 2002).

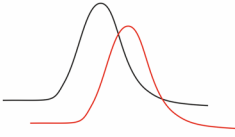
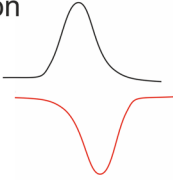
### Potassium

After the rainfall event,  $\text{K}^+$  exhibited a peak at the time EC started to decrease (T3) (Fig. 5). A significant positive correlation was found between  $\text{K}^+$  and discharge, Mg, Na, Cr, Cu, As, Rb, Cs, Ba, Gd, Dy, Ho, Er, Tm, Yb, and all particle sizes. A significant negative correlation was found with pH and  $\text{NO}_3^-$  (Fig. 4).

Similar to  $\text{Cl}^-$ , the mobilization of  $\text{K}^+$  was observed after the rainfall event, which hints toward a transport mechanism of  $\text{K}^+$  from the land surface into the aquifer. This is consistent with earlier studies that had identified  $\text{K}^+$  as an effective tracer for storm runoff (Mahler et al. 2008). Besides a natural origin (Hem 1985),  $\text{K}^+$  is considered as an indicator of



**Fig. 6** Additional overview over parameters measured at the spring that were mobilized and diluted after the rainfall event, including the respective increase or decrease in comparison to the baseline, either as % or as factor (for all increases larger than 100%)

Observation	Parameter
<b>Mobilization</b> 	all particle sizes (mean $\times 7.2$ ), <i>E. coli</i> ( $\times 120$ ), Coliforms ( $\times 61$ ), $\text{Cl}^-$ (+42%), $\text{K}^+$ (+83%), Gd ( $\times 3.6$ ), $\text{Na}^+$ (+58%), $\text{Al}^3+$ (+75%), V (+24%), Cr (+33%), $\text{Mn}^{2+}$ (+75%), $\text{Fe}^{2+}$ (+70%), As (+13%), Rb (+68%), Sr (+9%), La* (+31%), $\text{Ce}^{3+}$ (+72%), Pr* ( $\times 2.9$ ), $\text{Nd}^{3+}$ (+34%), $\text{Sm}^{3+}$ ( $\times 5.0$ ), $\text{Eu}^{3+}$ ( $\times 7.7$ ), Tb* (+39%), Dy (+53%), Ho (+49%), Er (+44%), Tm (+45%), Yb (+49%), Lu (+47%)  <i>*peak several days later than the other parameters</i>
<b>Dilution</b> 	EC (-1%), $\text{HCO}_3^-$ (-8%), $\text{Ca}^{2+}$ (-24%), $\text{NO}_3^-$ (-18%), $\text{SO}_4^{2-}$ (-17%), $\text{Mg}^{2+}$ (-23%), Li (-29%)

wastewater in rivers and karst springs, as  $\text{K}^+$  is a major constituent of urine and often associated with other wastewater indicators such as carbamazepine or acesulfame (Nödler et al. 2011; Yin et al. 2019; Hamdan et al. 2020; Buss and Achten 2022). This hypothesis of WWTP being a source for  $\text{K}^+$  is supported by the mobilization and positive correlation with fecal bacteria, Gd, and Rb during the rainfall event.

Another possible source for  $\text{K}^+$  are K-containing fertilizers (Skowron et al. 2018; Murrell et al. 2021), which may play a minor role during the monitored rainfall event as  $\text{K}^+$  showed an opposed behavior to the  $\text{NO}_3^-$  of agricultural origin (strong negative correlation). Nevertheless, the behavior of  $\text{K}^+$  could differ during another rainfall event and  $\text{K}^+$  is likely, though to a lesser extent, also originating from fertilizers and manure which are applied to agricultural land within the catchment area (Mahler et al 2008).

### Gadolinium

Gd showed a fivefold increase in concentrations after the rainfall event, with mean concentrations of 10.7 ng/L and a range of 5.1–28.2 ng/L (Table 2 and Fig. 5). Thus, Gd showed a strong variation after the rainfall event, covering a similar concentration range as the annual samples but within approximately one week. Gd concentrations showed a strong positive anomaly of  $\text{Gd}/\text{Gd}^* = 3.7$  (with a range of  $\text{Gd}/\text{Gd}^* = 2.2$  to  $\text{Gd}/\text{Gd}^* = 8.3$ ), when standardized with PAAS, whereas the strongest positive anomalies occurred during the Gd peak. For event samples Gd, showed a significant positive correlation with discharge, coliforms and *E. coli*,  $\text{Na}^+$ ,  $\text{K}^+$ , Cr, Cu, As, Rb, Cs, Dy, Ho, Er, Tm, Yb, Lu, and all

particle sizes. A significant negative correlation was found with pH,  $\text{HCO}_3^-$ ,  $\text{NO}_3^-$ , Ca, Mn, and U (Fig. 4).

Results show clear mobilization and transport of Gd through the aquifer, similar to  $\text{K}^+$  and  $\text{Cl}^-$ . One likely cause could be sewer overflows, that regularly occur during heavy rainfall events. This would explain the fast arrival (time lag of 78 h) but relatively short peak of Gd following the rainfall event and highlights transport through highly karstified conduits.

Moreover, the strong positive Gd anomaly during the Gd peak hints at an anthropogenic source (Bau and Dulski 1996), where Gd is also considered to be an indicator of wastewater contamination (Knappe et al. 2005). There are several rainwater retention basins established in the catchment, which can potentially overflow if the water storage capacity is exceeded (municipality Laichingen 2022). In such cases a mixture of wastewater and rainwater is directly released into the karst system, leading to a significant pollution of the groundwater resources.

Mobilization of Gd during the rainfall event, indicates (at least partial) retention of Gd by the WWTPs during regular operation (no sewer overflow). The input of Gd into the sewer system is assumed to be more or less constant at all times. Thus, if the WWTPs would directly release all received Gd into the karst system without treatment, Gd would have been diluted but not mobilized. In contrast to other studies (Macke et al. 2021; Laczovics et al. 2023) WWTPs in the catchment operate activated carbon filters, which may have led to a noticeable removal of Gd containing MRI contrasting agents, which is suggested by laboratory experiments (Rashad et al. 2017;

Elizalde-González et al. 2017). Furthermore, Gd could also be removed during other treatment steps in the WWTP or concentrations before the rainfall event could have been generally lower due to weekly variations.

### Fecal bacteria – *E. coli*

*E. coli* numbers show a strong increase after the rainfall event, with maximum concentrations of 17,168 MPN/100 mL (95% confidence interval from 11,233 to 24,360 MPN/100mL). These very high numbers of *E. coli* show strong positive correlations with discharge, temperature, Na<sup>+</sup>, Sm, Eu, Gd, Tb, Dy, Ho, Er, Tm, Yb, Lu, Th, and all particle sizes, and a weaker positive correlation with K<sup>+</sup> and Rb.

During the rainfall event, *E. coli* demonstrated an extremely high mobilization with an approximately 120-fold increase compared to baseline concentrations (Table 2 and Fig. 5). As fecal bacteria originate from the land surface, they are flushed into the aquifer by infiltrating precipitation or surface water (Mahler et al. 2000; Knierim et al. 2015). Measured values are very high in comparison to other karst springs with up to 3973 MPN/100 mL (e.g., Pronk et al. 2007; Frank et al. 2022; Schachner-Gröhs et al. 2023) which is similar to wastewater-impacted karst springs with little to no wastewater treatment measures which contained *E. coli* numbers up to approximately 10,000–24,000 MPN/100 mL (Ender et al. 2017; Richter et al. 2021).

A similar observation has been made for a smaller karst spring 50 km south-west from Blautopf, where *E. coli* numbers increased up to 10<sup>3</sup>–10<sup>4</sup> colony forming units (CFU) in 100 mL, which was an increase up to four orders of magnitude compared to baseline conditions, as a result of sewer overflow (Heinz et al. 2009). Furthermore, the hypothesis of a sewer overflow is additionally supported by the positive correlation with Gd, K<sup>+</sup>, and Rb which are wastewater indicators (Choubert et al. 2011; Knappe et al. 2005) and septic tanks as well as treated wastewater are typical sources for fecal bacteria (Katz et al. 2009; Knierim et al. 2015).

*E. coli* numbers return to baseline conditions after approximately five days, implicating a very strong but short-lived contamination event for this karst spring, where transport occurs through well-established conduits. Nevertheless, such high and fast occurring contamination events often contain

high rates of pathogens (e.g., viruses and bacteria) and can pose a significant problem to the overall water quality and management of a karst spring (Flynn and Sinreich 2010; Butscher et al. 2011). In particular untreated wastewater, as a potential source, typically contains a wide range of other contaminants (Mahler et al. 2000; Kovačič and Ravbar 2005; Brown et al. 2011). The high temporal variability further underlines the importance of intensive monitoring of water quality in karst aquifers (Mahler et al. 2000).

Manure can also provide a possible source for fecal coliforms (Kelly et al. 2009) which cannot be completely excluded, although a positive correlation with Na<sup>+</sup>, Cl<sup>−</sup>, and K<sup>+</sup> would also be expected in this case. In the context of heavy rainfall events, *E. coli* are often transported through karst aquifers, whereas a distinction of origin is often difficult in catchments with mixed land use. Furthermore, *E. coli* bacteria can be stored in the epikarst during dryer conditions and be flushed out by a following rainfall event (Knierim et al. 2015; Buckerfield et al. 2019).

### Particle counts

Particle counts were measured throughout the rainfall event and show approximately a 3.5-fold increase in the course of the rainfall event (e.g., for 1 µm particles) (Table 3 and Fig. 5). A significant strong positive correlation was found between all particle sizes (1–25 µm) and discharge, K<sup>+</sup>, Cr, As, Rb, Cs, and Gd. Smaller particle sizes (<10 µm) in particular, showed a strong positive correlation with Dy, Ho, Er, Tm, and Yb. Fecal bacteria showed a positive but weaker correlation with all particle sizes, especially for smaller diameters (Fig. 4).

Particle counts are in general rather sensitive with respect to changing hydrological conditions, e.g., increasing flow velocities and turbulence inside the conduits, that mobilize particles both from within the cave system (autochthonous) and from the surface (allochthonous) (Pronk et al. 2009). In the present study, the presence of fecal bacteria coincided with high particle counts, but not necessarily vice versa, e.g., particles counts were high for autochthonous turbidity as well (Fig. 5), but were not associated with *E. coli*. The correlation between particle counts and fecal bacteria is somewhat blurred, as the hydrological reaction of the spring is complex. It is noteworthy

**Table 3** Mean, minimum, maximum, and median particle counts per mL during event sampling in 2021

Statistic	Unit	Particle size diameter									
		1 µm	2 µm	3 µm	4 µm	5 µm	6 µm	7 µm	8 µm	9 µm	10 µm
Mean	particles/mL	2382	963	401	198	139	73	43	29	23	23
Min	particles/mL	1316	530	216	102	66	34	18	10	8	6
Max	particles/mL	4530	2003	911	477	394	235	165	136	121	167
Median	particles/mL	2124	814	330	156	107	55	33	22	18	17

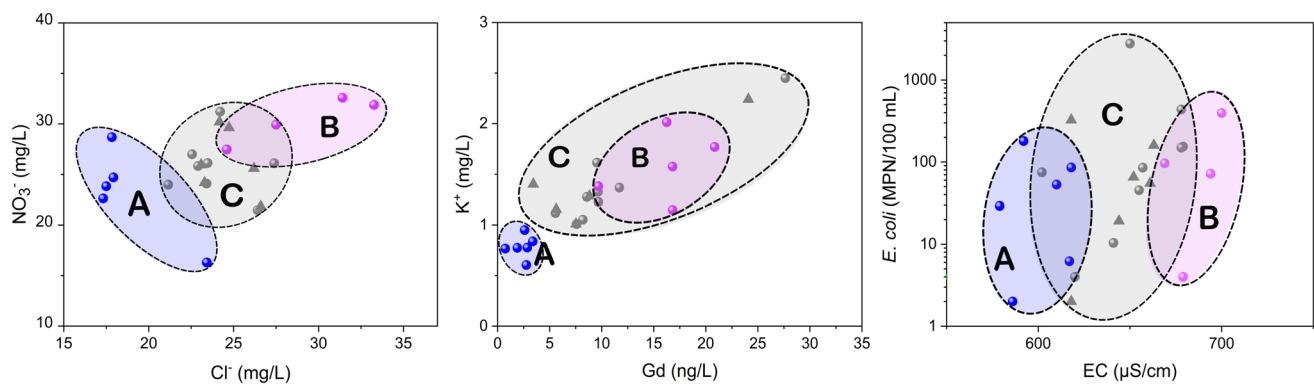


**Fig. 7** Selected parameters for cave samples at different sampling dates in SCa (sampling point A) and SCb (sampling point B). Sampling point C contains water from SCa and SCb, whereas gray triangles indicate samples from the cave lake and gray dots indicate sam-

ples from the spring. The cave lake and the spring are connected by a single conduit without branches. Please note the logarithmic scale for *E. coli* bacteria

that during T3 (allochthonous) 1  $\mu\text{m}$  particles increased alongside fecal bacteria, whereas 10  $\mu\text{m}$  particles gradually decreased. Furthermore, the increase in bacterial numbers (approximately 100-fold) was far stronger than the increase in particles numbers (3.5-fold increase). Turbidity showed a similar pattern to particle counts during the rainfall event but measured values were very low (maximum concentrations during rainfall event reached 0.29 NTU) in contrast to the high fecal contamination, suggesting individual particle counts by diameter to be a better approximation than turbidity. Turbidity and particle counts, particularly in the small-diameter range, may be able to serve as indicator parameters for bacterial contamination (Pronk et al. 2007; Ender et al. 2017), which could be supported for the investigated rainfall event, where small particles ( $<10 \mu\text{m}$ ) seem to serve as a proxy for the occurrence of fecal contamination, but do not provide information on the intensity of contamination. However, the correlation between turbidity or particle counts as an indicator for fecal contamination is less pronounced for smaller precipitation events (Buckfield et al. 2019). Moreover, the particles themselves can serve as transport vectors for pathogens and organic contaminants and are therefore relevant for water quality assessment (Vesper et al. 2001).

Hydrochemical responses after the rainfall event could be linked primarily to anthropogenic sources. Especially the input of nutrients and contaminants through point infiltration during heavy rainfall is of particular relevance for strong changes of the water quality of karst aquifers.

Occurrence of heavy rainfall events are projected to increase in future climate scenarios (Tabari 2020). As described above, intensive precipitation events often result in a strong reaction of the hydrograph and therefore exhibit a rapid and strong contamination transport with pronounced

surface-derived input (Tobin et al. 2021; Ravbar et al. 2023). Especially strong temporal changes and short transit times, enhancing the viability of viruses and bacteria, are of particular relevance to comprehensively assess the vulnerability of karst springs (Flynn and Sinreich 2010; Leins et al. 2025). The individual hydrographic response and vulnerability of karst springs to changing precipitation patterns is nevertheless complex and depends on the season, as well as site-specific and preceding conditions (Ravbar et al. 2023; Leins et al. 2025). A thick epikarst, which plays an important role in storage of water and contaminants (Vesper et al. 2001; Aquilina et al. 2006; Mahler and Massei 2007), can buffer increasing changes in precipitation, but to a lesser extent than other aquifers (Liesch and Wunsch 2019; Filipini et al. 2024).

### Spatial resolution and paired-catchment approach

To apply the paired-catchment approach to a subsurface karst and cave system, the catchment area was divided into two sub-catchments, each containing an independent branch of the cave system. Water samples were taken at different time intervals, depending on the accessibility of caves, in SCa (sampling point A), SCb (sampling point B) and in a cave lake that already contains water from both sub-catchments (sampling point C) (Fig. 1). As sampling point C (cave lake) and the spring are connected by a single conduit without in- or outflow, samples from the spring are included for better visibility under section C as well (gray dots, Fig. 7). Concentrations of selected parameters are given in Table 2 and Fig. 7.

Mean values for the cave lake (point C) and the spring were comparable (Table 2 and Fig. 7) and can be described as a mixture of both sub-catchments.

SCa and SCb contribute a similar amount to the discharge of the Blautopf Spring (Lauber et al. 2014). Discharge measurements performed on two consecutive days yielded a discharge of 323 L/s for SCa and 271 L/s for SCb (September 2023) during a discharge of 564–604 L/s at the spring, confirming the balanced contribution of discharge.

EC in samples from SCa was in all cases lower (mean 600  $\mu\text{S}/\text{cm}$ ) than in SCb (mean 686  $\mu\text{S}/\text{cm}$ ) (Fig. 7), indicating a higher general input of ions from SCb to Blautopf Spring. As samples were taken during different days, EC could furthermore be influenced by short-term hydrologic and seasonal variations and contributions from dissolved geogenic compounds such as  $\text{Ca}^{2+}$  or  $\text{Mg}^{2+}$  (Goldscheider and Drew 2007); however, the variation in geogenic contributions is likely low as both sub-catchments share the same geology, morphology, and climate.

$\text{Cl}^-$  concentrations in SCb were higher than in SCa, taking into account the behavior during the rainfall event, the WWTPs located in SCb are a likely point-source for  $\text{Cl}^-$ . Owing to similar geologic conditions between sampling sites, geogenic  $\text{Cl}^-$  is likely to play a minor role in the significant concentration differences. However, as there were no cave samples taken during snow melt, the impact of road salt could lead to more equal concentrations of  $\text{Cl}^-$  in both sub-catchments during winter time. Interestingly, despite the expected input of  $\text{Cl}^-$  from agriculture (Kelly et al. 2009), which is present in both sub-catchments, the concentrations of  $\text{Cl}^-$  in SCb were higher. These concentration differences underline WWTP effluents as an additional source.

$\text{NO}_3^-$  concentrations in SCb showed on average higher concentrations than SCa (Table 2 and Fig. 7). The ratio of agriculture in SCa is approximately 50% in contrast to 68% in SCb, indicating a likely higher  $\text{NO}_3^-$  application in SCb. The distinguishable difference in  $\text{NO}_3^-$  concentration in both sub-catchments approximately reflects the differing ratio of agriculture. Agriculture is a major input factor for  $\text{NO}_3^-$  into karst aquifers (Smith et al. 2020). Therefore, the paired-catchment approach can in this case be applied very well for  $\text{NO}_3^-$ , even though agriculture is found in both sub-catchments. Nevertheless, this is only valid assuming a similar application on all agricultural areas.

Similar to  $\text{Cl}^-$ ,  $\text{K}^+$  concentrations were also always higher in SCb (Table 2 and Fig. 7). A likely and continuous source of  $\text{K}^+$  can be WWTP effluents, which do not change annually (Nödler et al. 2011). Nevertheless, SCb also has a higher proportion of agriculture (68% in contrast to 50% in SCa) and thus an influence from  $\text{K}^+$  containing fertilizers and manure (Skowron et al. 2018; Murrell et al. 2021) may play a secondary, less pronounced role (as described for  $\text{Cl}^-$ ). However, these ratios might change for samples taken shortly after the fertilization of agricultural fields (Wang et al. 2022).

Gd concentrations showed a strong difference between SCa (mean 2.4 ng/L) and sevenfold higher concentrations in SCb (mean 16.1 ng/L) (Table 2 and Fig. 7). Samples from SCb moreover showed a strong positive Gd anomaly (mean  $\text{Gd}/\text{Gd}^* = 5.1$ ).

Water samples from SCa only show a negligible anthropogenic influence based on Gd anomalies, with Gd concentrations being similar to uncontaminated groundwater samples where typical concentration values of 1–3 ng/L are reported globally (Ebrahimi and Barbieri 2019). In contrast, high Gd concentrations, including a strong positive anomaly in SCb, clearly show a strong anthropogenic influence. Gd has been identified as a “powerful indicator” (Boester and Rüde 2020) for groundwater/surface water interaction as Gd is considered to be a tracer for WWTP effluents, as Gd is poorly removed by many WWTPs (Möller et al. 2000; Brinjes et al. 2016; De Paula Marteleto and Enzweiler 2021). Results from this study support the use of Gd as an indicator for the presence of WWTP effluents in karst systems; however, it also mentions a potential retaining of Gd by WWTPs with activate carbon filters during normal operation.

Fecal bacteria were found in all samples (annual samples, event samples, cave samples) but in varying concentrations and with only a slight difference between SCa and SCb. The ubiquitously occurring fecal bacteria in both sub-catchments are likely related both to WWTP effluents and to the application of manure (Kelly et al. 2009), as livestock are present in the catchment area throughout the year. The relevance of both sources may change depending on hydrological conditions, whether a sewer overflow is occurring, and on the timing of manure application.

Observations from both sub-catchments were compared with a sample collected from a nearby WWTP effluent, which discharges solely into SCb. The WWTP effluent showed strongly elevated concentrations in EC (844  $\mu\text{S}/\text{cm}$ ),  $\text{Cl}^-$  (127.4 mg/L),  $\text{K}^+$  (20.35 mg/L), *E. coli* (4978 MPN/100 mL), and Gd (236 ng/L), including an extremely strong positive Gd anomaly of  $\text{Gd}/\text{Gd}^* = 295.2$  emphasizing the anthropogenic input. Gd concentrations are in the range of globally investigated effluents of WWTPs (30 to 845 ng/L) (Ebrahimi and Barbieri 2019; Laczovics et al. 2023). WWTP effluents are thus considered to be a driving factor of elevated concentrations of the listed ions in SCb. Furthermore, the WWTP effluent contained comparatively low  $\text{NO}_3^-$  concentrations at the sampling date with 12.55 mg/L, supporting the primarily agricultural input of  $\text{NO}_3^-$  in the spring catchment.

For the catchment area of Blautopf Spring, the primary source of contamination is anthropogenic and originates from the land surface. SCb has a significantly higher contribution to contaminant transport due to the higher percentage of agriculture and two WWTPs in the catchment, compared to SCa.



By transferring the paired-catchment approach to the subsurface of one catchment, it was possible to assess the impact of local land use impacts in higher spatial resolution. Cave streams in each sub-catchment represent chemical parameters for only one part of the catchment and a clear differentiation could be made despite coarse sampling intervals at different dates. In contrast to previous paired-catchment studies (Zhao et al. 2010; Salavati et al. 2016; Smith et al. 2020; Bai et al. 2024) which compared two individual catchments, the approach presented here is even more independent of geology, morphology, and climate as only one catchment is investigated. This is especially interesting to gain a differentiated insight into localized and potentially seasonal land use impacts and parameter variations within larger karst aquifers, for which it is often difficult to find a matching catchment for a classical paired-catchment approach (van Loon et al. 2019). This new approach would further help to understand processes inside the aquifer that cannot always be fully understood by only investigating parameters at the spring outlet (Hartmann et al. 2011). The origin of individual components can be investigated, both from point- and diffuse infiltration, as shown by parameters related to wastewater effluents and agriculture. However, there are also some restrictions for the application of this approach, e.g., if the catchment is too small, does not allow for spatially distributed sampling of different cave streams, catchment size, and location in unknown or if land use is very similar over the whole catchment area and parameters can thus not be differentiated. Tracer tests could additionally be used to identify unknown flow connections in cave streams and their relative contributions to spring discharge (Goldscheider et al. 2008), which information is required to differentiate localized land use impacts.

This subsurface paired-catchment approach, which was exemplary tested at the Blautopf catchment, could also be tested in other karst aquifers as a new method to assess spatially resolved land use impacts and support a better understanding of localized sources and input factors, as contaminants from the surface can have a detrimental impact on the water quality of karst springs (e.g., Vesper et al. 2001). Moreover, changes in land use and land cover which can impact the water quality and quantity of karst aquifers (Nguyet and Goldscheider 2006; Sarker and Fryar 2022; Zhang et al. 2023a; Leins et al. 2025) could be assessed with this approach. Localized monitoring during rainfall events might help to reveal detailed transport processes within the karst aquifer. The subsurface paired-catchment approach could be a beneficial data base for groundwater models in karst systems that often suffer from a lack of localized information inside the aquifer system (Hartmann et al. 2011, 2013).

## Conclusions

Short- and long-term changes in water quality were investigated at a large karst spring in Southern Germany (Blautopf) which was monitored during a 30-month period and also intensively sampled during a rainfall event. The spring catchment was further divided into two sub-catchments which have an identical geology, morphology, and climate but with different land use and cave systems. These prerequisites allowed transferring the paired-catchment approach to the subsurface, for the first time, and to draw conclusions on the impacts of land use by spatially resolved investigation of the water quality. This modified application of the paired-catchment approach could open up new possibilities, in particular for larger karst aquifers with accessible cave systems, to assess the local impacts of land use.

Most parameters do not show a pronounced and systematic seasonal variation for the long-term monitoring. Major findings were that  $\text{NO}_3^-$  variations reflected the fertilizing of crops during springtime, whereas  $\text{Cl}^-$  concentrations were highest during winter and springtime, due to the application of road salt.

Water quality parameters showed strong changes in response to a heavy rainfall event, but quickly returned to baseline conditions thereafter within a couple of days. This is typical for well-developed karst systems as a result of rapid transport in large conduits. The main observations include:

- *E. coli* increased drastically (up to 17,000 MPN/100 mL) during the rainfall event, with  $\text{Cl}^-$ ,  $\text{K}^+$ , and Gd also showing strong mobilization, which could likely be linked to a sewer overflow caused by heavy precipitation.
- $\text{NO}_3^-$  showed a clear dilution effect and was mainly linked to chemical fertilizers and to a lesser extent to the application of manure, as a positive correlation between  $\text{NO}_3^-$  and *E. coli* could not be detected.
- The increase in particle counts was simultaneous with *E. coli* numbers, emphasizing the applicability of particle counts (especially with small diameters  $\approx 1 \mu\text{m}$ ) as an indicator for fecal contamination.
- Particle counts showed two distinct peaks during the rainfall event, allowing a clear distinction between autochthonous and allochthonous sources of turbidity.

Furthermore, a paired-catchment approach was demonstrated to be successfully applied, for the first time, to a subsurface karst and cave system. Both sub-catchments showed clearly distinguishable differences in the water quality that could be related to the respective land use in the catchment as the geological background, morphology, and climatic conditions were directly comparable:



- $\text{Cl}^-$  could be linked to anthropogenic sources like WWTP effluents and potentially agriculture.
- $\text{NO}_3^-$  showed higher concentrations for the sub-catchment with higher proportion of agriculture.
- $\text{K}^+$  and Gd (with strong positive Gd anomalies) were found to serve as viable tracers for (treated) wastewater. Nevertheless, continuous but moderately elevated Gd concentrations at the spring support a partial removal of Gd by WWTPs.

For Blautopf Spring the parameters described above revealed human activities to be the primary factor impacting water quality in the karst aquifer. In particular, unregulated discharge of untreated wastewater into karst aquifers poses a significant risk to groundwater quality. As heavy rainfall events are predicted to increase in the context of climate change (Tabari 2020), the contamination from sewer overflows and overall fast contaminant transport may become more frequent in the future. The combination of spatial and temporal water sampling proved to be a powerful methodology to identify impacts of land use activities on the water quality in karst springs. The necessity for close-knit monitoring of karst springs is highlighted, as individual parameters might behave differently under varying hydrological conditions (Ravbar et al. 2023). In particular the transfer of a paired-catchment approach to the subsurface (cave system) proved to be a useful tool to assess spatially differentiated impacts of land use in karst aquifers, even at coarse sampling intervals. An application of the subsurface paired-catchment approach on other karst aquifers could be very interesting to gain insight into hydrochemical processes inside the aquifer, which could serve as a valuable data source for hydrological models that often lack this information (Hartmann et al. 2011).

**Acknowledgements** We would like to thank the local caving clubs ARGE Blautopf and ARGE Blaukarst very much for their great support and cooperation throughout the entire project. We also thank the local WWTP for allowing a sampling opportunity and for providing additional information. A special thanks goes to the Cave Association Laichingen for welcoming and hosting us during field work. We especially thank Markus Klotz for support with the particle counter and the bypass. A special thanks goes also to the city of Blaubeuren, which allowed the setup of a monitoring station at the spring and in the associated building. We are further grateful for the background information on WWTP provided by Alb-Donau District. The authors would especially like to acknowledge the persistent support from the hydrogeology laboratory staff, namely Daniela Blank, Chris Buschhaus and Christine Roske-Stegemann. For providing discharge data we thank the State Environmental Agency of Baden-Wuerttemberg (LUBW). This publication has further been prepared using the European Union's Copernicus Land Monitoring Service information. We moreover thank the three anonymous reviewers for their valuable comments on our manuscript.

**Author contribution** NG and NG wrote the research proposal and supervised the project. All authors contributed to the overall study conception, design, and planning. YKM carried out field work, data

collection, and data analysis. YKM wrote the manuscript and prepared the figures and tables, NG and NG provided input and regular feedback throughout the different stages of the study and critically reviewed the manuscript. All authors read and approved the final manuscript.

**Funding** Open Access funding enabled and organized by Projekt DEAL. The authors thank the German Research Foundation (DFG) for funding this study as part of the IMPART project (project number: 432288610). We further acknowledge support by the KIT-Publication Fund of the Karlsruhe Institute of Technology.

**Data Availability** Data are available upon reasonable request from the authors.

## Declarations

**Competing interests** The authors declare that they have no competing interests.

**Open Access** This article is licensed under a Creative Commons Attribution 4.0 International License, which permits use, sharing, adaptation, distribution and reproduction in any medium or format, as long as you give appropriate credit to the original author(s) and the source, provide a link to the Creative Commons licence, and indicate if changes were made. The images or other third party material in this article are included in the article's Creative Commons licence, unless indicated otherwise in a credit line to the material. If material is not included in the article's Creative Commons licence and your intended use is not permitted by statutory regulation or exceeds the permitted use, you will need to obtain permission directly from the copyright holder. To view a copy of this licence, visit <http://creativecommons.org/licenses/by/4.0/>.

## References

- Aide M, Nakajima T (2020) Rare earth elements and their minerals, 1st edn. IntechOpen, London, UK
- Andreo B, Goldscheider N, Vadillo I (2006) Karst groundwater protection: first application of a Pan-European approach to vulnerability, hazard and risk mapping in the Sierra de L  bar (Southern Spain). *Sci Total Environ* 357:54–73. <https://doi.org/10.1016/j.scitotenv.2005.05.019>
- Aquilina L, Ladouche B, D  rfliger N (2006) Water storage and transfer in the epikarst of karstic systems during high flow periods. *J Hydrol* 327:472–485. <https://doi.org/10.1016/j.jhydrol.2005.11.054>
- ARGE Blaukarst (2014) Hessenh  hle | Arbeitsgemeinschaft Blaukarst. <http://www.blauhoehle.de/category/hessenh  hle/>. Accessed 29 Apr 2025
- ARGE Blautopf (2020) Blauh  hle. <http://www.blauhoehle.org/>. Accessed 29 April 2025
- Bai X, Liu W, Wang T et al (2024) Large-sample detection of reservoir impacts on flow regime alteration through improved paired-catchment approach. *J Hydrol* 642:131872. <https://doi.org/10.1016/j.jhydrol.2024.131872>
- Bakalowicz M (2005) Karst groundwater: a challenge for new resources. *Hydrogeol J* 13:148–160. <https://doi.org/10.1007/s10040-004-0402-9>
- Bakalowicz M (2004) The epikarst, the skin of karst. In: Epikarst: Proceedings of the Symposium Held October 1 through 4, 2003 Shepherdstown, West Virginia. Karst Waters Institute, Shepherdstown, West Virginia, USA

- Baraza T, Hasenmueller EA (2021) Road salt retention and transport through vadose zone soils to shallow groundwater. *Sci Total Environ* 755:142240. <https://doi.org/10.1016/j.scitotenv.2020.142240>
- Bau M, Dulski P (1996) Anthropogenic origin of positive gadolinium anomalies in river waters. *Earth Planet Sci Lett* 143:245–255. [https://doi.org/10.1016/0012-821X\(96\)00127-6](https://doi.org/10.1016/0012-821X(96)00127-6)
- Boester U, Rüde TR (2020) Utilize gadolinium as environmental tracer for surface water-groundwater interaction in karst. *J Contam Hydrol* 235:103710. <https://doi.org/10.1016/j.jconhyd.2020.103710>
- Böhlke J-K (2002) Groundwater recharge and agricultural contamination. *Hydrogeol J* 10:153–179. <https://doi.org/10.1007/s10040-001-0183-3>
- Brown AE, Zhang L, McMahon TA et al (2005) A review of paired catchment studies for determining changes in water yield resulting from alterations in vegetation. *J Hydrol* 310:28–61. <https://doi.org/10.1016/j.jhydrol.2004.12.010>
- Brown J, Bach L, Aldous A et al (2011) Groundwater-dependent ecosystems in Oregon: an assessment of their distribution and associated threats. *Front Ecol Environ* 9:97–102. <https://doi.org/10.1890/090108>
- Brünjes R, Bichler A, Hoehn P et al (2016) Anthropogenic gadolinium as a transient tracer for investigating river bank filtration. *Sci Total Environ* 571:1432–40. <https://doi.org/10.1016/j.scitotenv.2016.06.105>
- Buckerfield SJ, Quilliam RS, Waldron S et al (2019) Rainfall-driven *E. coli* transfer to the stream-conduit network observed through increasing spatial scales in mixed land-use paddy farming karst terrain. *Water Research X* 5:100038. <https://doi.org/10.1016/j.wroa.2019.100038>
- Buss J, Achten C (2022) Spatiotemporal variations of surface water quality in a medium-sized river catchment (Northwestern Germany) with agricultural and urban land use over a five-year period with extremely dry summers. *Sci Total Environ* 818:151730. <https://doi.org/10.1016/j.scitotenv.2021.151730>
- Butscher C, Auckenthaler A, Scheidler S, Huggenberger P (2011) Validation of a numerical indicator of microbial contamination for karst springs. *Ground Water* 49:66–76. <https://doi.org/10.1111/j.1745-6584.2010.00687.x>
- Caetano Bicalho C, Batiot-Guilhe C, Seidel JL et al (2012) Geochemical evidence of water source characterization and hydrodynamic responses in a karst aquifer. *J Hydrol* 450–451:206–218. <https://doi.org/10.1016/j.jhydrol.2012.04.059>
- Chen Z, Auler AS, Bakalowicz M et al (2017) The world Karst Aquifer Mapping project: concept, mapping procedure and map of Europe. *Hydrogeol J* 25:771–785. <https://doi.org/10.1007/s10040-016-1519-3>
- Cho KH, Han D, Park Y et al (2010) Evaluation of the relationship between two different methods for enumeration fecal indicator bacteria: colony-forming unit and most probable number. *J Environ Sci (China)* 22:846–850. [https://doi.org/10.1016/s1001-0742\(09\)60187-x](https://doi.org/10.1016/s1001-0742(09)60187-x)
- Cholet C, Steinmann M, Charlier J-B, Denimal S (2019) Characterizing fluxes of trace metals related to dissolved and suspended matter during a storm event: application to a karst aquifer using trace metals and rare earth elements as provenance indicators. *Hydrogeol J* 27:305–319. <https://doi.org/10.1007/s10040-018-1859-2>
- Choubert J-M, Pomiès M, Martin Ruel S, Coquery M (2011) Influent concentrations and removal performances of metals through municipal wastewater treatment processes. *Water Sci Technol* 63:1967–1973. <https://doi.org/10.2166/wst.2011.126>
- De Paula Marteleto T, Enzweiler J (2021) Anthropogenic gadolinium as a tracer of raw sewage in surface water. *Environ Earth Sci* 80:607. <https://doi.org/10.1007/s12665-021-09903-0>
- Doummar J, Geyer T, Baierl M et al (2014) Carbamazepine breakthrough as indicator for specific vulnerability of karst springs: application on the Jeita spring, Lebanon. *Appl Geochem* 47:150–156. <https://doi.org/10.1016/j.apgeochem.2014.06.004>
- Ebrahimi P, Barbieri M (2019) Gadolinium as an Emerging Microcontaminant in Water Resources: Threats and Opportunities. *Geosci* 9:93. <https://doi.org/10.3390/geosciences9020093>
- Elizalde-González MP, García-Díaz E, González-Perea M, Mattusch J (2017) Removal of gadolinium-based contrast agents: adsorption on activated carbon. *Environ Sci Pollut Res* 24:8164–8175. <https://doi.org/10.1007/s11356-017-8491-x>
- Ender A, Goeppert N, Grimmeisen F, Goldscheider N (2017) Evaluation of  $\beta$ -d-glucuronidase and particle-size distribution for microbiological water quality monitoring in Northern Vietnam. *Sci Total Environ* 580:996–1006. <https://doi.org/10.1016/j.scitotenv.2016.12.054>
- European Union (2020) Directive (EU) 2020/2184 of the European Parliament and of the Council of 16 December 2020 on the quality of water intended for human consumption (recast)
- Fan X, Goeppert N, Goldscheider N (2023) Quantifying the historic and future response of karst spring discharge to climate variability and change at a snow-influenced temperate catchment in central Europe. *Hydrogeol J* 31:2213–2229. <https://doi.org/10.1007/s10040-023-02703-9>
- Filippini M, Segadelli S, Dinelli E et al (2024) Hydrogeological assessment of a major spring discharging from a calcarenitic aquifer with implications on resilience to climate change. *Sci Total Environ* 913:169770. <https://doi.org/10.1016/j.scitotenv.2023.169770>
- Flynn RM, Sinreich M (2010) Characterisation of virus transport and attenuation in epikarst using short pulse and prolonged injection multi-tracer testing. *Water Res* 44:1138–49. <https://doi.org/10.1016/j.watres.2009.11.032>
- Frank S, Fahrmeier N, Goeppert N, Goldscheider N (2022) High-resolution multi-parameter monitoring of microbial water quality and particles at two alpine karst springs as a basis for an early-warning system. *Hydrogeol J* 30:2285–2298. <https://doi.org/10.1007/s10040-022-02556-8>
- Goldscheider N, Drew D (2007) *Methods in Karst Hydrogeology*, 1st edn. Taylor & Francis, London, UK
- Goldscheider N, Meiman J, Pronk M, Smart C (2008) Tracer tests in karst hydrogeology and speleology. *Int J Speleol* 37:27–40. <https://doi.org/10.5038/1827-806X.37.1.3>
- Goldscheider N (2019) A holistic approach to groundwater protection and ecosystem services in karst terrains. *Carbonates Evaporites* 34:1241–1249. <https://doi.org/10.1007/s13146-019-00492-5>
- Grimmeisen F, Lehmann MF, Liesch T (2017) Isotopic constraints on water source mixing, network leakage and contamination in an urban groundwater system. *Sci Total Environ* 583:202–213. <https://doi.org/10.1016/j.scitotenv.2017.01.054>
- Gutiérrez F, Parise M, De Waele J, Jourde H (2014) A review on natural and human-induced geohazards and impacts in karst. *Earth-Sci Rev* 138:61–88. <https://doi.org/10.1016/j.earscirev.2014.08.002>
- Hamdan I, Licha T, Toll M et al (2020) Quantification of wastewater pollution load using potassium concentrations in karst spring discharges. *Environ Earth Sci* 79:402. <https://doi.org/10.1007/s12665-020-09145-6>
- Hankin B, Page TJC, Chappell NA et al (2021) Using micro-catchment experiments for multi-local scale modelling of nature-based solutions. *Hydrol Process* 35:e14418. <https://doi.org/10.1002/hyp.14418>
- Hartmann A, Kralik M, Humer F et al (2011) Identification of a karst system's intrinsic hydrodynamic parameters: upscaling from single springs to the whole aquifer. *Environ Earth Sci* 65:2377–2389. <https://doi.org/10.1007/s12665-011-1033-9>
- Hartmann A, Weiler M, Wagener T et al (2013) Process-based karst modelling to relate hydrodynamic and hydrochemical characteristics to system properties. *Hydrol Earth Syst Sci* 17:3305–3321. <https://doi.org/10.5194/hess-17-3305-2013>

- Heinz B, Birk S, Liedl R et al (2009) Water quality deterioration at a karst spring (Gallusquelle, Germany) due to combined sewer overflow: evidence of bacterial and micro-pollutant contamination. *Environ Geol* 57:797–808. <https://doi.org/10.1007/s00254-008-1359-0>
- Hem JD (1985) Study and Interpretation of the Chemical Characteristics of Natural Water. U. S. Geological Survey, Alexandria, VA, USA
- Hibbert AR (1967) Forest treatment effects on water yield. In: Sopper WW, Lull HW (eds) International Symposium on Forest Hydrology. Pergamon Press, Oxford, UK, pp 527–543
- Huang B, Yuan Z, Li D et al (2020) Effects of soil particle size on the adsorption, distribution, and migration behaviors of heavy metal(loid)s in soil: a review. *Environ Sci Process Impacts* 22:1596–1615. <https://doi.org/10.1039/d0em00189a>
- Huebsch M, Fenton O, Horan B (2014) Mobilisation or dilution? Nitrate response of karst springs to high rainfall events. *Hydrol Earth Syst Sci* 18:4423–4435. <https://doi.org/10.5194/hess-18-4423-2014>
- Husic A, Fox J, Adams E (2019) Nitrate pathways, processes, and timing in an agricultural Karst system: development and application of a numerical model. *Water Resour Res* 55:2079–2103. <https://doi.org/10.1029/2018WR023703>
- IDEXX (2025) MPN Generator Software - IDEXX US. <https://www.idexx.com/en/water/resources/mpn-generator/>. Accessed 15 Aug 2025
- Iyad N, S.Ahmad M, Alkhatib SG, Hjouj M (2023) Gadolinium contrast agents- challenges and opportunities of a multidisciplinary approach: literature review. *Eur J Radiol* 11:100503. <https://doi.org/10.1016/j.ejro.2023.100503>
- Jakeman AJ, Barreteau O, Hunt RJ (2016) Integrated Groundwater Management. Springer International Publishing, Cham
- Jang J, Hur H-G, Sadowsky MJ (2017) Environmental *Escherichia coli*: ecology and public health implications—a review. *J Appl Microbiol* 123:570–581. <https://doi.org/10.1111/jam.13468>
- Jiang S, Ibáñez JSP, Wu Y, Zhang J (2021) Geochemical tracers in submarine groundwater discharge research: practice and challenges from a view of climate changes. *Environ Rev* 29:242–259. <https://doi.org/10.1139/er-2020-0093>
- Katz BG, Griffin DW, Davis JH (2009) Groundwater quality impacts from the land application of treated municipal wastewater in a large karstic spring basin: chemical and microbiological indicators. *Sci Total Environ* 407:2872–2886. <https://doi.org/10.1016/j.scitotenv.2009.01.022>
- Kelly WR, Panno SV, Hackley KC et al (2009) Bacteria contamination of groundwater in a mixed land-use Karst region. *Water Expo Health* 1:69–78. <https://doi.org/10.1007/s12403-009-0006-7>
- Knappe A, Möller P, Dulski P, Pekdeger A (2005) Positive gadolinium anomaly in surface water and ground water of the urban area Berlin, Germany. *Geochemistry* 65:167–189. <https://doi.org/10.1016/j.chemer.2004.08.004>
- Knierim KJ, Hays PD, Bowman D (2015) Quantifying the variability in *Escherichia coli* (*E. coli*) throughout storm events at a karst spring in northwestern Arkansas, United States. *Environ Earth Sci* 74(6):4607–4623. <https://doi.org/10.1007/s12665-015-4416-5>
- Kovačič G, Ravbar N (2005) A review of the potential and actual sources of pollution to groundwater in selected karst areas in Slovenia. *Nat Hazards Earth Syst Sci* 5:225–233. <https://doi.org/10.5194/nhess-5-225-2005>
- Laczovics A, Csige I, Szabó S et al (2023) Relationship between gadolinium-based MRI contrast agent consumption and anthropogenic gadolinium in the influent of a wastewater treatment plant. *Sci Total Environ* 877:162844. <https://doi.org/10.1016/j.scitotenv.2023.162844>
- LaMoreaux JW (2019) Environmental Geology: A Volume in the Encyclopedia of Sustainability Science and Technology, 2nd edn. Springer US, New York, NY
- Larocque M, Mangin A, Razack M, Banton O (1998) Contribution of correlation and spectral analyses to the regional study of a large karst aquifer (Charente, France). *J Hydrol* 205:217–231. [https://doi.org/10.1016/S0022-1694\(97\)00155-8](https://doi.org/10.1016/S0022-1694(97)00155-8)
- Lauber U, Ufrecht W, Goldscheider N (2014) Spatially resolved information on karst conduit flow from in-cave dye tracing. *Hydrol Earth Syst Sci* 18:435–445. <https://doi.org/10.5194/hess-18-435-2014>
- Leal Filho W, Kotter R, Özuyar PG et al (2023) Understanding rare earth elements as critical raw materials. *Sustainability* 15:1919. <https://doi.org/10.3390/su15031919>
- Leins T, Scheller M, Özdemir Çallı K et al (2025) A new process-based approach for defining karst aquifer vulnerability to contamination risks under global changes. *Sci Total Environ* 966:178561. <https://doi.org/10.1016/j.scitotenv.2025.178561>
- Liesch T, Wunsch A (2019) Aquifer responses to long-term climatic periodicities. *J Hydrol* 572:226–242. <https://doi.org/10.1016/j.jhydrol.2019.02.060>
- Long DT, Voice TC, Niagolova ND, McElmurry SP (2012) Effects of human activities on karst groundwater geochemistry in a rural area in the Balkans. *Appl Geochem* 27:1920–1931. <https://doi.org/10.1016/j.apgeochem.2012.07.003>
- Luo M, Wan L, Liao C (2023) Geographic and transport controls of temperature response in karst springs. *J Hydrol* 623:129850. <https://doi.org/10.1016/j.jhydrol.2023.129850>
- Macke M, Quarles CD, Sperling M, Karst U (2021) Fast and automated monitoring of gadolinium-based contrast agents in surface waters. *Water Res* 207:117836. <https://doi.org/10.1016/j.watres.2021.117836>
- Mahler B, Massei N (2007) Anthropogenic contaminants as tracers in an urbanizing karst aquifer. *J Contam Hydrol* 91:81–106. <https://doi.org/10.1016/j.jconhyd.2006.08.010>
- Mahler BJ, Garner BD (2009) Using nitrate to quantify quick flow in a Karst aquifer. *Ground Water* 47:350–360. <https://doi.org/10.1111/j.1745-6584.2008.00499.x>
- Mahler BJ, Personné J-C, Lods GF, Drogue C (2000) Transport of free and particulate-associated bacteria in karst. *J Hydrol* 238:179–193. [https://doi.org/10.1016/S0022-1694\(00\)00324-3](https://doi.org/10.1016/S0022-1694(00)00324-3)
- Mahler BJ, Valdes D, Musgrove M, Massei N (2008) Nutrient dynamics as indicators of karst processes: comparison of the Chalk aquifer (Normandy, France) and the Edwards aquifer (Texas, U.S.A.). *J Contam Hydrol* 98:36–49. <https://doi.org/10.1016/j.jconhyd.2008.02.006>
- McLennan SM (2001) Relationships between the trace element composition of sedimentary rocks and upper continental crust. *Geochim Geophys Geosyst* 2:2000GC000109. <https://doi.org/10.1029/2000GC000109>
- Mohaghegh Motlagh A, Yang Z (2019) Detection and occurrence of indicator organisms and pathogens. *Water Environ Res* 91:1402–1408. <https://doi.org/10.1002/wer.1238>
- Möller P, Dulski P, Bau M et al (2000) Anthropogenic gadolinium as a conservative tracer in hydrology. *J Geochem Explor* 69–70:409–414. [https://doi.org/10.1016/S0375-6742\(00\)00083-2](https://doi.org/10.1016/S0375-6742(00)00083-2)
- Murrell TS, Mikkelsen RL, Sulewski G (2021) Improving Potassium Recommendations for Agricultural Crops. Springer International Publishing, Cham
- Neary D (2016) Long-term forest paired catchment studies: what do they tell us that landscape-level monitoring does not? *Forests* 7:164. <https://doi.org/10.3390/f7080164>
- Nguyet VTM, Goldscheider N (2006) A simplified methodology for mapping groundwater vulnerability and contamination risk, and



- its first application in a tropical karst area, Vietnam. *Hydrogeol J* 14:1666–1675. <https://doi.org/10.1007/s10040-006-0069-5>
- Nödler K, Licha T, Fischer S et al (2011) A case study on the correlation of micro-contaminants and potassium in the Leine River (Germany). *Appl Geochem* 26:2172–2180. <https://doi.org/10.1016/j.apgeochem.2011.08.001>
- Overbo A, Heger S, Gulliver J (2021) Evaluation of chloride contributions from major point and nonpoint sources in a northern U.S. state. *Sci Total Environ* 764:144179. <https://doi.org/10.1016/j.scitotenv.2020.144179>
- Perera N, Gharabaghi B, Noehammer P, Kilgour B (2010) Road salt application in Highland Creek Watershed, Toronto, Ontario - chloride mass balance. *Water Qual Res J* 45:451–461. <https://doi.org/10.2166/wqrj.2010.044>
- Perrin J, Jeannin P-Y, Zwahlen F (2003) Epikarst storage in a karst aquifer: a conceptual model based on isotopic data, Milandre test site, Switzerland. *J Hydrol* 279:106–124. [https://doi.org/10.1016/S0022-1694\(03\)00171-9](https://doi.org/10.1016/S0022-1694(03)00171-9)
- Pinaut J-L, Plagnes V, Aquilina L, Bakalowicz M (2001) Inverse modeling of the hydrological and the hydrochemical behavior of hydrosystems: characterization of Karst system functioning. *Water Resour Res* 37:2191–2204. <https://doi.org/10.1029/2001WR900018>
- Pronk M, Goldscheider N, Zopfi J (2007) Particle-size distribution as indicator for fecal bacteria contamination of drinking water from karst springs. *Environ Sci Technol* 41:8400–5. <https://doi.org/10.1021/es071976f>
- Pronk M, Goldscheider N, Zopfi J, Zwahlen F (2009) Percolation and particle transport in the unsaturated zone of a karst aquifer. *Ground Water* 47:361–9. <https://doi.org/10.1111/j.1745-6584.2008.00509.x>
- Pu J, Yuan D, Zhao H, Shen L (2014) Hydrochemical and PCO<sub>2</sub> variations of a cave stream in a subtropical karst area, Chongqing, SW China: piston effects, dilution effects, soil CO<sub>2</sub> and buffer effects. *Environ Earth Sci* 71:4039–4049. <https://doi.org/10.1007/s12665-013-2787-z>
- Rashad GM, Mahmoud MR, Sheha RR (2017) Impregnated activated carbon for the adsorption of Gd(III) radionuclides from aqueous solutions: Particulate Science and Technology: Vol 36, No 5. *Partic Sci Technol* 36:609–617
- Rantz SE (1982) Measurement and computation of streamflow: volume 1. Measurement of stage and discharge. USGS, Washington, D. C.
- Ravbar N, Engelhardt I, Goldscheider N (2011) Anomalous behaviour of specific electrical conductivity at a karst spring induced by variable catchment boundaries: the case of the Podstenjšek spring, Slovenia. *Hydrol Process* 25:2130–2140. <https://doi.org/10.1002/hyp.7966>
- Ravbar N, Mulec J, Mayaud C (2023) A comprehensive early warning system for karst water sources contamination risk, case study of the Unica springs, SW Slovenia. *Sci Total Environ* 885:163958. <https://doi.org/10.1016/j.scitotenv.2023.163958>
- Richter D, Goeppert N, Zindler B, Goldscheider N (2021) Spatial and temporal dynamics of suspended particles and *E. coli* in a complex surface-water and karst groundwater system as a basis for an adapted water protection scheme, northern Vietnam. *Hydrogeol J* 29:1965–1978. <https://doi.org/10.1007/s10040-021-02356-6>
- Robinson HK, Hasenmueller EA (2017) Transport of road salt contamination in karst aquifers and soils over multiple timescales. *Sci Total Environ* 603:94–108. <https://doi.org/10.1016/j.scitotenv.2017.05.244>
- Ryan M, Meiman J (1996) An examination of short-term variations in water quality at a karst spring in Kentucky. *Ground Water* 34:23–30. <https://doi.org/10.1111/j.1745-6584.1996.tb01861.x>
- Salavati B, Oudin L, Furusho-Percot C, Ribstein P (2016) Modeling approaches to detect land-use changes: Urbanization analyzed on a set of 43 US catchments. *J Hydrol* 538:138–151. <https://doi.org/10.1016/j.jhydrol.2016.04.010>
- Sarker SK, Fryar AE (2022) Characterizing hydrological functioning of three large karst springs in the Salem Plateau, Missouri, USA. *Hydrology* 9(6):96. <https://doi.org/10.3390/hydrology9060096>
- Schachner-Gröhs I, Strohhammer T, Frick C et al (2023) Low antimicrobial resistance in *Escherichia coli* isolates from two large Austrian alpine karstic spring catchments. *Sci Total Environ* 894:164949. <https://doi.org/10.1016/j.scitotenv.2023.164949>
- Selg M, Schwarz K (2009) Am Puls der schönen Lau – zur Hydrogeologie des Blautopf-Einzugsgebietes (*At the heart of beautiful Lau – the hydrogeology of the Blautopf catchment area*). *Laichinger Höhlenfreund* 44:45–72
- Skowron P, Skowrońska M, Bronowicka-Mielniczuk U et al (2018) Anthropogenic sources of potassium in surface water: the case study of the Bystrzyca river catchment, Poland. *Agric Ecosyst Environ* 265:454–460. <https://doi.org/10.1016/j.agee.2018.07.006>
- Smith DNI, Ortega-Camacho D, Acosta-González G et al (2020) A multi-approach assessment of land use effects on groundwater quality in a karstic aquifer. *Heliyon* 6:e03970. <https://doi.org/10.1016/j.heliyon.2020.e03970>
- Laichingen Stadtverwaltung (2022) Amtsblatt Laichinger Nachrichten (*official journal of the municipality of Laichingen*). *Stadtverwaltung Laichingen* 14:2
- Stevanović Z (2019) Karst waters in potable water supply: a global scale overview. *Environ Earth Sci* 78:1–12. <https://doi.org/10.1007/s12665-019-8670-9>
- Strebel O, Duynisveld WHM, Böttcher J (1989) Nitrate pollution of groundwater in western Europe. *Agric Ecosyst Environ* 26:189–214. [https://doi.org/10.1016/0167-8809\(89\)90013-3](https://doi.org/10.1016/0167-8809(89)90013-3)
- Sun J, Tang C, Wu P et al (2013) Hydrogeochemical characteristics of streams with and without acid mine drainage impacts: a paired catchment study in karst geology, SW China. *J Hydrol* 504:115–124. <https://doi.org/10.1016/j.jhydrol.2013.09.029>
- Tabari H (2020) Climate change impact on flood and extreme precipitation increases with water availability. *Sci Rep* 10:13768. <https://doi.org/10.1038/s41598-020-70816-2>
- Tobin BW, Polk JS, Arpin SM et al (2021) A conceptual model of epikarst processes across sites, seasons, and storm events. *J Hydrol* 596:125692. <https://doi.org/10.1016/j.jhydrol.2020.125692>
- Toran L, Reisch CE (2013) Using stormwater hysteresis to characterize karst spring discharge. *Ground Water* 51:575–587. <https://doi.org/10.1111/j.1745-6584.2012.00984.x>
- Tran DA, Goeppert N, Goldscheider N (2023) Use of major ion chemistry and trace and rare earth elements to characterize hydraulic relations, mixing processes and water–rock interaction in the Dong Van karst aquifer system, Northern Vietnam. *Hydrogeol J* 31(7):1735–1753. <https://doi.org/10.1007/s10040-023-02689-4>
- van Loon AF, Rangelcroft S, Coxon G et al (2019) Using paired catchments to quantify the human influence on hydrological droughts. *Hydrol Earth Syst Sci* 23:1725–1739. <https://doi.org/10.5194/hess-23-1725-2019>
- Vesper DJ, Loop CM, White WB (2001) Contaminant transport in karst aquifers. *TAK* 13:63–73
- Vesper DJ, White WB (2004) Spring and conduit sediments as storage reservoirs for heavy metals in karst aquifers. *Environ Geol* 45:481–493. <https://doi.org/10.1007/s00254-003-0899-6>
- Villinger E, Ufrecht W (1989) Ergebnisse neuer Markierungsversuche im Einzugsgebiet des Blautopfs (mittlere Schwäbische Alb) (*Results of new tracer tests in the Blautopf catchment (middle Swabian Alb)*). *Mitteilungen des Verbandes der Deutschen Höhlen- und Karstforscher eV* 35:25–38

- Visser A-N, Lehmann MF, Rügner H et al (2021) Fate of nitrate during groundwater recharge in a fractured karst aquifer in Southwest Germany. *Hydrogeol J*. <https://doi.org/10.1007/s10040-021-02314-2>
- Wang Z-J, Li S-L, Yue F-J et al (2020) Rainfall driven nitrate transport in agricultural karst surface river system: insight from high resolution hydrochemistry and nitrate isotopes. *Agric Ecosyst Environ* 291:106787. <https://doi.org/10.1016/j.agee.2019.106787>
- Wang Z-J, Yue F-J, Wang Y-C et al (2022) The effect of heavy rainfall events on nitrogen patterns in agricultural surface and underground streams and the implications for karst water quality protection. *Agric Water Manage* 266:107600. <https://doi.org/10.1016/j.agwat.2022.107600>
- Zhang P, Wang X-D, Yue F-J et al (2023) Dynamic characteristics of nitrogen transport in various land use in a typical karst catchment during rainfall events. *Environ Earth Sci* 82:332. <https://doi.org/10.1007/s12665-023-10980-6>
- Zhao M, Zeng C, Liu Z, Wang S (2010) Effect of different land use/land cover on karst hydrogeochemistry: a paired catchment study of Chenqi and Dengzhanhe, Puding, Guizhou, SW China. *J Hydrol* 388:121–130. <https://doi.org/10.1016/j.jhydrol.2010.04.03>
- Wang K, Chen X, Wu Z (2023) Traceability and biogeochemical process of nitrate in the Jinan Karst Spring Catchment, North China. *Water* 15:2718. <https://doi.org/10.3390/w15152718>
- Weber G, Kubiniok J (2022) Spring waters as an indicator of nitrate and pesticide pollution of rural watercourses from nonpoint sources: results of repeated monitoring campaigns since the early 2000s in the low mountain landscape of Saarland, Germany. *Environ Sci Eur* 34:53. <https://doi.org/10.1186/s12302-022-00632-0>
- White W (2015) Chemistry and karst. *Acta Carsologica* 44(3):349–362. <https://doi.org/10.3986/ac.v44i3.1896>
- Williams PW (1983) The role of the subcutaneous zone in karst hydrology. *J Hydrol* 61:45–67. [https://doi.org/10.1016/0022-1694\(83\)90234-2](https://doi.org/10.1016/0022-1694(83)90234-2)
- Wu Y, Wu Y, He P et al (2025) Spatial characteristics of soil potassium in the early stage of vegetation restoration and influencing factors in southwest China's karst region. *Sci Rep* 15:2106. <https://doi.org/10.1038/s41598-024-84576-w>
- Yin H, Xie M, Zhang L et al (2019) Identification of sewage markers to indicate sources of contamination: low cost options for misconnected non-stormwater source tracking in stormwater systems. *Sci Total Environ* 648:125–134. <https://doi.org/10.1016/j.scitotenv.2018.07.448>
- Yue F-J, Li S-L, Zhong J, Liu J (2018) Evaluation of factors driving seasonal nitrate variations in surface and underground systems of a karst catchment. *Vadose Zone J* 17(1):170071. <https://doi.org/10.2136/vzj2017.04.0071>
- Yue F-J, Waldron S, Li S-L et al (2019) Land use interacts with changes in catchment hydrology to generate chronic nitrate pollution in karst waters and strong seasonality in excess nitrate export. *Sci Total Environ* 696:134062. <https://doi.org/10.1016/j.scitotenv.2019.134062>
- Zhang J, Liesch T, Chen Z, Goldscheider N (2023) Global analysis of land-use changes in karst areas and the implications for water resources. *Hydrogeol J* 31:1197–1208. <https://doi.org/10.1007/s10040-023-02650-5>

**Publisher's Note** Springer Nature remains neutral with regard to jurisdictional claims in published maps and institutional affiliations.